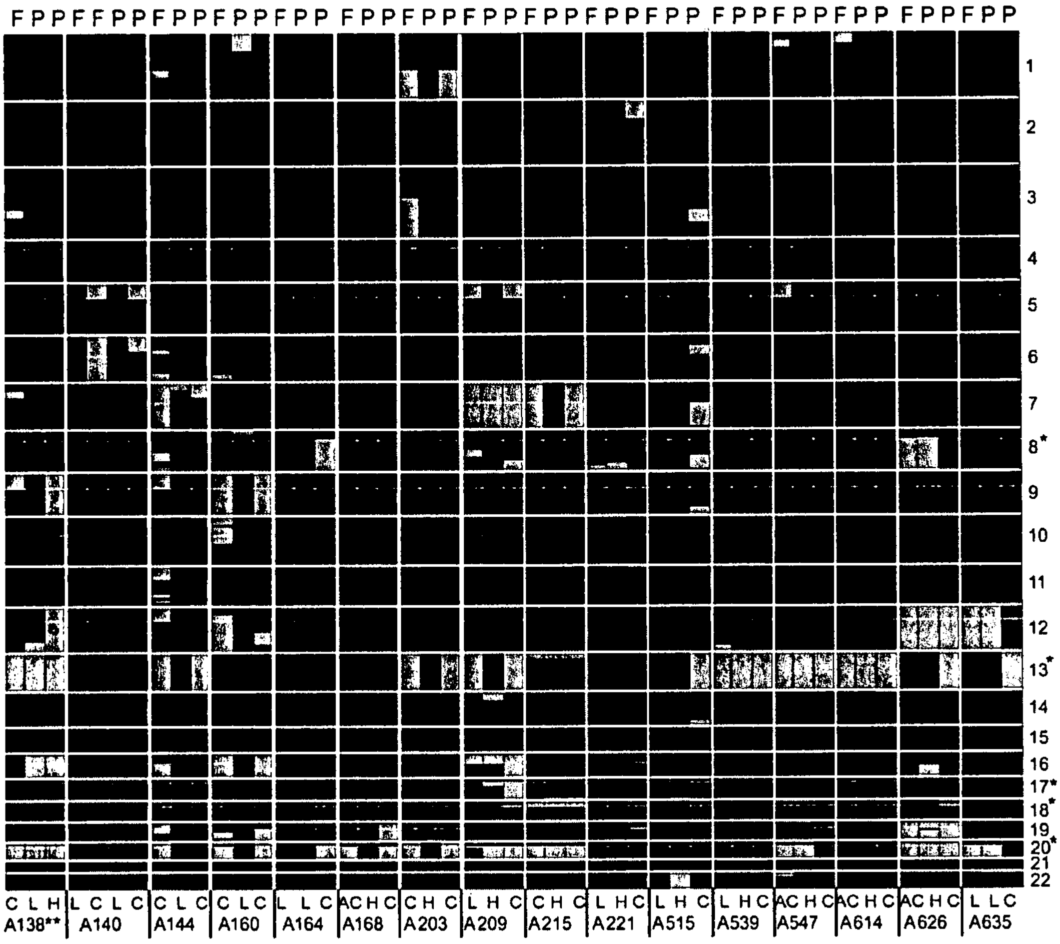

Figure 5. Overview of gains (green), physical losses (red), and copy number neutral LOH (blue) in adenoma and carcinoma fractions of 16 rectal tumour samples. On the *x*-axis are all the different samples, successively the frozen sample and the FFPE-adenoma and -carcinoma fractions. On the *y*-axis are the chromosomes. The five 'malignant aberrations' are indicated by an asterisk (*). Top of figure: F (frozen), P (paraffin-embedded). Bottom of figure: L (adenoma with low-grade dysplasia), H (adenoma with high-grade dysplasia), AC (mixture of adenoma and carcinoma), C (carcinoma). The carcinoma fraction in the FFPE tissue from sample A138 was too mall to analyse (**)

study are highly similar to those found in other studies; although part of the events identified would have been missed by CGH, owing to copy number neutral LOH [28,29]. Subsequently, logistic regression analysis was performed, and these five events together were shown to build a quantitative progression model of rectal tumourigenesis.

We found that rectal adenomas showed relatively few aberrations, while carcinomas showed many. However, exceptions were identified: adenomas with many aberrations and carcinomas with few aberrations. In adenoma fractions from cases with a carcinoma, twice the amount of such 'malignant aberrations' was observed, compared with pure adenomas. Furthermore, comparison of adenoma and carcinoma tissue from the same lesion, showed in the majority of cases (11/16) an increase of one to three of the 'malignant aberrations' in the carcinoma fraction. By comparing carcinomas with and without lymph node metastases, we discovered that lymph node positive cases demonstrated an amount of chromosomal aberrations that was similar to that in the lymph node negative cases. This indicates that genomic instability is an early event in the progression of rectal cancer, as has also been shown by others (reviewed in [49]). However, one remarkable difference was found: cases with lymph node metastasis more frequently showed a gain on 1q. In other studies a 1q gain has been related to metastases to the liver, but not to the lymph nodes [18,50]. Another study found a strong correlation between 8q23–24 gain and lymph node metastases [32]. However, we detected equal percentages of 8q gain in the carcinoma with and without lymph node metastases. The gain on 1q and a possible relation to lymph node metastasis needs further validation in a larger series. Currently, expression array analysis is performed on the same samples, and both data types are integrated. These combined data might reveal novel markers for lymph node metastasis.

A strength of this study concerns the homogeneity of the sample collection. All samples were obtained from rectal tumours, while previous studies usually

described a heterogeneous group of colon, rectum, and sigmoid tumours. Several recent papers have indicated differences between colonic and rectal cancer and have advocated that when prognostic markers are investigated, differences between tumour location should be considered [34,35].

This study did not take tumour heterogeneity into account. As is known from the literature, colorectal cancers are heterogeneous [51–54]. We currently study chromosomal instability in different biopsies to determine tumour heterogeneity. Initial results indicate that three biopsies reliably represent the genomic aberrations. Five out of 18 tumours showed heterogeneity, displayed by extra chromosomal aberrations in one or two biopsies.

In conclusion, a compilation of five carcinoma-specific events can accurately distinguish adenomas from carcinomas. In contrast to pure adenomas, adenoma fractions of carcinoma cases already carry 'malignant aberrations'. Such results might complement clinical data to guide treatment selection more precisely, although thorough prospective validation in independent series is still required.

Acknowledgements

We thank the PATHAN (Rotterdam) and SSDZ (Delft) for providing the tissue samples, A Middeldorp for control samples, and Dr F Graadt van Roggen for critical reading of the manuscript. This project was supported by Dutch Cancer Society grant RUL 2003-2807.

Supplementary material

Supplementary material may be found at the web address http://www.interscience.wiley.com/jpages/0022-3417/suppmat/path.2180.html

References

1. Kapiteijn E, Marijnen CA, Nagtegaal ID, Putter H, Steup WH, Wiggers T, *et al.* Preoperative radiotherapy combined with total mesorectal excision for resectable rectal cancer. *N Engl J Med* 2001;**345**:638–646.
2. Peeters KC, van de Velde CJ, Leer JW, Martijn H, Junggeburt JM, Kranenbarg EK, *et al.* Late side effects of short-course preoperative radiotherapy combined with total mesorectal excision for rectal cancer: increased bowel dysfunction in irradiated patients — a Dutch colorectal cancer group study. *J Clin Oncol* 2005;**23**:6199–6206.
3. Buess G, Mentges B, Manncke K, Starlinger M, Becker HD. Technique and results of transanal endoscopic microsurgery in early rectal cancer. *Am J Surg* 1992;**163**:63–69.
4. de Graaf EJ, Doornebosch PG, Stassen LP, Debets JM, Tetteroo GW, Hop WC. Transanal endoscopic microsurgery for rectal cancer. *Eur J Cancer* 2002;**38**:904–910.
5. Rokke O, Iversen KB, Ovrebo K, Maartmann-Moe H, Skarstein A, Halvorsen JF. Local resection of rectal tumors by transanal endoscopic microsurgery: experience with the first 70 cases. *Dig Surg* 2005;**22**:182–189.
6. Casadesus D. Transanal endoscopic microsurgery: a review. *Endoscopy* 2006;**38**:418–423.
7. Ganai S, Kanumuri P, Rao RS, Alexander AI. Local recurrence after transanal endoscopic microsurgery for rectal polyps and early cancers. *Ann Surg Oncol* 2006;**13**:547–556.
8. Maslekar S, Beral DL, White TJ, Pillinger SH, Monson JR. Transanal endoscopic microsurgery: where are we now? *Dig Surg* 2006;**23**:12–22.
9. Sakamoto GD, MacKeigan JM, Senagore AJ. Transanal excision of large, rectal villous adenomas. *Dis Colon Rectum* 1991;**34**:880–885.
10. Sengupta S, Tjandra JJ. Local excision of rectal cancer: what is the evidence? *Dis Colon Rectum* 2001;**44**:1345–1361.
11. Floyd ND, Saclarides TJ. Transanal endoscopic microsurgical resection of pT1 rectal tumors. *Dis Colon Rectum* 2006;**49**:164–168.
12. Guerrieri M, Baldarelli M, Morino M, Trompetto M, Da Rold A, Selmi I, *et al.* Transanal endoscopic microsurgery in rectal adenomas: experience of six Italian centres. *Dig Liver Dis* 2006;**38**:202–207.
13. Nastro P, Beral D, Hartley J, Monson JR. Local excision of rectal cancer: review of literature. *Dig Surg* 2005;**22**:6–15.
14. Stipa F, Burza A, Lucandri G, Ferri M, Pigazzi A, Ziparo V, *et al.* Outcomes for early rectal cancer managed with transanal endoscopic microsurgery: a 5-year follow-up study. *Surg Endosc* 2006;**20**:541–545.
15. Hermanek P, Gall FP. Early (microinvasive) colorectal carcinoma. Pathology, diagnosis, surgical treatment. *Int J Colorectal Dis* 1986;**1**:79–84.
16. Balmain A, Gray J, Ponder B. The genetics and genomics of cancer. *Nat Genet* 2003;**33**:(Suppl): 238–244.
17. Lanza G Jr, Maestri I, Dubini A, Gafa R, Santini A, Ferretti S, *et al.* p53 expression in colorectal cancer: relation to tumor type, DNA ploidy pattern and short-term survival. *Am J Clin Pathol* 1996;**105**:604–612.
18. Diep CB, Kleivi K, Ribeiro FR, Teixeira MR, Lindgjaerde OC, Lothe RA. The order of genetic events associated with colorectal cancer progression inferred from meta-analysis of copy number changes. *Genes Chromosomes Cancer* 2006;**45**:31–41.
19. Grade M, Ghadimi BM, Varma S, Simon R, Wangsa D, Barenboim-Stapleton L, *et al.* Aneuploidy-dependent massive deregulation of the cellular transcriptome and apparent divergence of the Wnt/beta-catenin signaling pathway in human rectal carcinomas. *Cancer Res* 2006;**66**:267–282.
20. Hermsen M, Postma C, Baak J, Weiss M, Rapallo A, Sciutto A, *et al.* Colorectal adenoma to carcinoma progression follows multiple pathways of chromosomal instability. *Gastroenterology* 2002;**123**:1109–1119.
21. Hoglund M, Gisselsson D, Hansen GB, Sall T, Mitelman F, Nilbert M. Dissecting karyotypic patterns in colorectal tumors: two distinct but overlapping pathways in the adenoma-carcinoma transition. *Cancer Res* 2002;**62**:5939–5946.
22. Ried T, Knutzen R, Steinbeck R, Blegen H, Schrock E, Heselmeyer K, *et al.* Comparative genomic hybridization reveals a specific pattern of chromosomal gains and losses during the genesis of colorectal tumors. *Genes Chromosomes Cancer* 1996;**15**:234–245.
23. Sugai T, Takahashi H, Habano W, Nakamura S, Sato K, Orii S, *et al.* Analysis of genetic alterations, classified according to their DNA ploidy pattern, in the progression of colorectal adenomas and early colorectal carcinomas. *J Pathol* 2003;**200**:168–176.
24. Thiagalingam S, Laken S, Willson JK, Markowitz SD, Kinzler KW, Vogelstein B, *et al.* Mechanisms underlying losses of heterozygosity in human colorectal cancers. *Proc Natl Acad Sci USA* 2001;**98**:2698–2702.
25. Huang J, Wei W, Zhang J, Liu G, Bignell GR, Stratton MR, *et al.* Whole genome DNA copy number changes identified by high density oligonucleotide arrays. *Hum Genomics* 2004;**1**:287–299.
26. Lieberfarb ME, Lin M, Lechpammer M, Li C, Tanenbaum DM, Febbo PG, *et al.* Genome-wide loss of heterozygosity analysis from laser capture microdissected prostate cancer using single nucleotide polymorphic allele (SNP) arrays and a novel bioinformatics platform dChipSNP. *Cancer Res* 2003;**63**:4781–4785.

27. Zhao X, Li C, Paez JG, Chin K, Janne PA, Chen TH, *et al.* An integrated view of copy number and allelic alterations in the cancer genome using single nucleotide polymorphism arrays. *Cancer Res* 2004;**64**:3060–3071.
28. Bignell GR, Huang J, Greshock J, Watt S, Butler A, West S, *et al.* High-resolution analysis of DNA copy number using oligonucleotide microarrays. *Genome Res* 2004;**14**:287–295.
29. Calhoun ES, Gallmeier E, Cunningham SC, Eshleman JR, Hruban RH, Kern SE. Copy-number methods dramatically underestimate loss of heterozygosity in cancer. *Genes Chromosomes Cancer* 2006;**45**:1070–1071.
30. Bardi G, Fenger C, Johansson B, Mitelman F, Heim S. Tumor karyotype predicts clinical outcome in colorectal cancer patients. *J Clin Oncol* 2004;**22**:2623–2634.
31. Leslie A, Stewart A, Baty DU, Mechan D, McGreavey L, Smith G, *et al.* Chromosomal changes in colorectal adenomas: relationship to gene mutations and potential for clinical utility. *Genes Chromosomes Cancer* 2006;**45**:126–135.
32. Ghadimi BM, Grade M, Liersch T, Langer C, Siemer A, Fuzesi L, *et al.* Gain of chromosome 8q23-24 is a predictive marker for lymph node positivity in colorectal cancer. *Clin Cancer Res* 2003;**9**:1808–1814.
33. Anwar S, Frayling IM, Scott NA, Carlson GL. Systematic review of genetic influences on the prognosis of colorectal cancer. *Br J Surg* 2004;**91**:1275–1291.
34. Kapiteijn E, Liefers GJ, Los LC, Kranenbarg EK, Hermans J, Tollenaar RA, *et al.* Mechanisms of oncogenesis in colon versus rectal cancer. *J Pathol* 2001;**195**:171–178.
35. Frattini M, Balestra D, Suardi S, Oggionni M, Alberici P, Radice P, *et al.* Different genetic features associated with colon and rectal carcinogenesis. *Clin Cancer Res* 2004;**10**(Pt 1):4015–4021.
36. Beart RW, Melton LJ III, Maruta M, Dockerty MB, Frydenberg HB, O'Fallon WM. Trends in right and left-sided colon cancer. *Dis Colon Rectum* 1983;**26**:393–398.
37. Scott N, Sagar P, Stewart J, Blair GE, Dixon MF, Quirke P. p53 in colorectal cancer: clinicopathological correlation and prognostic significance. *Br J Cancer* 1991;**63**:317–319.
38. Thibodeau SN, Bren G, Schaid D. Microsatellite instability in cancer of the proximal colon. *Science* 1993;**260**:816–819.
39. Rex DK, Ulbright TM, Cummings OW. Coming to terms with pathologists over colon polyps with cancer or high-grade dysplasia. *J Clin Gastroenterol* 2005;**39**:1–3.
40. West AB, Mitsuhashi T. Cancer or high-grade dysplasia? The present status of the application of the terms in colonic polyps. *J Clin Gastroenterol* 2005;**39**:4–6.
41. Miller SA, Dykes DD, Polesky HF. A simple salting out procedure for extracting DNA from human nucleated cells. *Nucleic Acids Res* 1988;**16**:1215.
42. Matsuzaki H, Loi H, Dong S, Tsai YY, Fang J, Law J, *et al.* Parallel genotyping of over 10,000 SNPs using a one-primer assay on a high-density oligonucleotide array. *Genome Res* 2004;**14**:414–425.
43. Lin M, Wei LJ, Sellers WR, Lieberfarb M, Wong WH, Li C. dChipSNP: significance curve and clustering of SNP-array-based loss-of-heterozygosity data. *Bioinformatics* 2004;**20**:1233–1240.
44. Eilers PH, de Menezes RX. Quantile smoothing of array CGH data. *Bioinformatics* 2005;**21**:1146–1153.
45. Nannya Y, Sanada M, Nakazaki K, Hosoya N, Wang L, Hangaishi A, *et al.* A robust algorithm for copy number detection using high-density oligonucleotide single nucleotide polymorphism genotyping arrays. *Cancer Res* 2005;**65**:6071–6079.
46. Lips EH, Dierssen JW, van Eijk R, Oosting J, Eilers PH, Tollenaar RA, *et al.* Reliable high-throughput genotyping and loss-of-heterozygosity detection in formalin-fixed, paraffin-embedded tumors using single nucleotide polymorphism arrays. *Cancer Res* 2005;**65**:10188–10191.
47. Knijnenburg J, Szuhai K, Giltay J, Molenaar L, Sloos W, Poot M, *et al.* Insights from genomic microarrays into structural chromosome rearrangements. *Am J Med Genet A* 2005;**132**:36–40.
48. Oosting J, Lips EH, van Eijk R, Eilers PH, Szuhai K, Wijmenga C, *et al.* High-resolution copy number analysis of paraffin-embedded archival tissue using SNP BeadArrays. *Genome Res* 2007.
49. Rajagopalan H, Nowak MA, Vogelstein B, Lengauer C. The significance of unstable chromosomes in colorectal cancer. *Nat Rev Cancer* 2003;**3**:695–701.
50. Knosel T, Schluns K, Stein U, Schwabe H, Schlag PM, Dietel M, *et al.* Chromosomal alterations during lymphatic and liver metastasis formation of colorectal cancer. *Neoplasia* 2004;**6**:23–28.
51. Bartos JD, Stoler DL, Matsui S, Swede H, Willmott LJ, Sait SN, *et al.* Genomic heterogeneity and instability in colorectal cancer: spectral karyotyping, glutathione transferase-M1 and ras. *Mutat Res* 2004;**568**:283–292.
52. Di Vinci A, Infusini E, Peveri C, Sciutto A, Orecchia R, Geido E, *et al.* Intratumor heterogeneity of chromosome 1, 7, 17, and 18 aneusomies obtained by FISH and association with flow cytometric DNA index in human colorectal adenocarcinomas. *Cytometry* 1999;**35**:369–375.
53. Saraga E, Bautista D, Dorta G, Chaubert P, Martin P, Sordat B, *et al.* Genetic heterogeneity in sporadic colorectal adenomas. *J Pathol* 1997;**181**:281–286.
54. Tollenaar RA, Bonsing BA, Kuipers-Dijkshoorn NJ, Hermans J, van de Velde CJ, Cornelisse CJ, *et al.* Evidence of clonal divergence in colorectal carcinoma. *Cancer* 1997;**79**:1304–1314.

Journal of Pathology
J Pathol 2008; **214**: 65–74
Published online 31 October 2007 in Wiley InterScience
(www.interscience.wiley.com) **DOI:** 10.1002/path.2258

Original Paper

The *CD30* gene promoter microsatellite binds transcription factor Yin Yang 1 (YY1) and shows genetic instability in anaplastic large cell lymphoma

M Franchina,[1] AJ Woo,[2] J Dods,[2] M Karimi,[1,2] D Ho,[2] T Watanabe,[3] DV Spagnolo[4] and LJ Abraham[2]*

[1] *Western Australian Institute for Medical Research & Centre for Medical Research, The University of Western Australia, Crawley, Western Australia*
[2] *School of Biomedical, Biomolecular and Chemical Sciences, University of Western Australia, Crawley, Western Australia*
[3] *Laboratory of Tumor Cell Biology, Department of Medical Genome Sciences, Graduate School of Frontier Sciences, University of Tokyo, 4-6-1 Shirokanedai, Minato-ku, Tokyo 108-109, Japan*
[4] *PathWest Laboratory Medicine WA and School of Surgery and Pathology, University of Western Australia, Crawley, Western Australia*

*Correspondence to:
LJ Abraham, Biochemistry and Molecular Biology, M310, School of Biomedical, Biomolecular and Chemical Sciences, University of Western Australia, 35 Stirling Highway, Crawley 6009, Western Australia.
E-mail: labraham@cyllene.uwa.edu.au

No conflicts of interest were declared.

Received: 16 April 2007
Revised: 7 August 2007
Accepted: 7 September 2007

Abstract

CD30 is a member of the TNF receptor family. Our interest lies in understanding the control of CD30 expression, particularly as its over-expression provides a diagnostic marker for a subset of non-Hodgkin's lymphomas, particularly anaplastic large cell lymphoma (ALCL), and because anti-CD30 treatment has been shown to be efficacious. We have identified a number of regulatory regions, including an Sp1 element in the minimal promoter, and a downstream promoter element that is required for start site selection. The discovery of both an activating AP1 site and an upstream microsatellite that represses transcriptional activity of CD30 suggests that this region is involved in dysregulation of CD30 expression. We have now identified the major microsatellite binding activity as transcription factor Yin Yang 1 by both one-hybrid cDNA library screening and peptide mass fingerprinting. Due to the strong repressive effect of the microsatellite, we also investigated whether microsatellite instability may induce changes in CD30 expression and hence explain the over-expression of CD30 in ALCL. Laser capture microdissection of ALCL biopsies and CD30 microsatellite typing indicated that the neoplastic cells show a high degree of variation, but this does not correlate with high CD30 expression seen in ALCL.

Keywords: **genetic instability; transcription factor; CD30; anaplastic large cell lymphoma**

Introduction

CD30 was first identified as a surface marker on Hodgkin and Reed–Sternberg cells of Hodgkin's lymphoma (HL) [1,2]. CD30 also is expressed in a variety of non-Hodgkin lymphomas (NHL) and reaches the highest frequency of expression in anaplastic large cell lymphoma (ALCL) [3]. The mechanism(s) underlying deregulated expression of CD30 in lymphoma is unknown, but the effects of over-expression may be explained in part by divergent CD30 signal transduction through the TNFR-associated factors (TRAFs) [4,5]. Signals emanating from CD30 diverge downstream of TRAF-2, leading to activation of NF-κB and c-Jun. Constitutive activation of NF-κB-RelA prevents Hodgkin/Reed–Sternberg (H/RS) cells in HL from undergoing apoptosis, whilst HL cell lines depleted of constitutive NF-κB are no longer able to produce tumours in immunodeficient mice [6]. In contrast, NF-κB activation is blocked in ALCL cells harbouring the ALK/NPM translocation, despite the high levels of CD30 expression [7]. The NPM-ALK oncoprotein impedes NF-κB activation following CD30 activation, by TRAF2's association with NPM-ALK [8].

The antiproliferative effect of CD30 activation on ALCL lines has been investigated for its potential therapeutic application. It has been shown that activation of CD30 by an unconjugated agonist antibody causes lymphoma regression and prolongs survival of immunodeficient mice xenografted with human systemic CD30$^+$ ALCL [9]. Clinically, increased levels of the CD30 ligand are associated with spontaneous regression of skin lesions in primary CD30$^+$ cutaneous lymphomas [10]. These and other studies indicate that expression of CD30 antigen is not only an important diagnostic and prognostic marker in ALCL but could also be useful as a target of novel therapies [11,12].

Although the downstream events that result from CD30 stimulation are becoming clearer, almost nothing is known about the processes that give rise to the high levels of CD30 seen in these lymphomas. Our hypothesis is that the mechanism of over-expression

of CD30 in ALCL involves the increased transcriptional activity of the *CD30* gene. As a step towards understanding what these upstream events are at the transcriptional level, we sought to identify the transcription factors that regulate the *CD30* gene in neoplastic cells. We have previously characterized the CD30 promoter [13] and a comparison of human and mouse *CD30* genes revealed significant identity, with both genes lacking consensus TATA box sequences but sharing conserved Sp1 and downstream initiator (DPE) elements [14]. We and others have identified other important transcriptional elements upstream of the transcriptional start-site, including Sp1 and ETS transcription factor binding sites [14,15]. We also identified a microsatellite CCAT repeat (CD30-MS) that was able to repress transcription from the CD30 promoter [14]. Given the importance of the CD30-MS as a transcriptional repressor, in this study we have determined the identity of the transcription factor(s) that are able to bind to this sequence and mediate repression of CD30 transcription.

Further studies indicate a marked degree of polymorphism in the CD30-MS [16–18]. The results prompted us to propose that deletion of the CD30-MS, due to mitotic instability, may promote a neoplastic phenotype in $CD30^+$ T cell lymphoma by relieving transcriptional repression, resulting in increased CD30 expression [14]. We also have tested the notion that microsatellite deletion was correlated with CD30 expression level, using a panel of CD30-expressing cell lines derived from HL and NHL [19]. However, there did not appear to be any direct relationship between microsatellite length and CD30 expression level. Because of the inherent accumulation of genomic aberations in cell lines, in the current study we assessed CD30 microsatellite instability in lymph node biopsies. Laser capture microdissections of $CD30^+$ and $CD30^-$ cells from ALCL lymph nodes were used in PCR to assess correlations between CD30-MS lengths and CD30 expression levels in individual cells.

Materials and methods

Cell line culture and transfection

Cell lines were obtained from the German Collection of Microorganisms and Cell Cultures (Braunschweig, Germany) and propagated in RPMI 1640 medium with L-glutamine, supplemented with 10% v/v heat-inactivated fetal bovine serum (FBS), 100 IU/ml penicillin and 100 μg/ml streptomycin (Invitrogen Australia Pty Ltd, Australia), at 37 °C in 5% CO_2.

Transfections were carried out using Lipofectamine 2000™ (Invitrogen) according to the manufacturer's instructions for Jurkat cells. Cells were subcultured 24 h prior to transfection without antibiotics and harvested at 8×10^5 cells/ml. After transfection, the cells were incubated at 37 °C for 24 h. Luciferase activity was measured using the Dual Luciferase Assay kit (Promega Corporation, Madison, WI). When required, qualified siRNA duplexes were obtained commercially (Smartpool siRNAs, Dharmacon Inc., Lafayette, CO, USA), fluorescently labelled with Cyanin3 dye and 1 nmol/ml used in transfection.

Electrophoretic mobility shift assay (EMSA)

Nuclear extracts were prepared as described previously [14]. For some experiments, S300-fractionated Jurkat extracts were used (see [20]). For EMSA, nuclear extracts (5 μg crude extract or 1 μg fractionated extract) were preincubated on ice for 10 min, together with 1 μg poly dI-dC. When required, 500 ng YY1 or Sp1 antibodies (Santa Cruz Biotechnology Inc., Santa Cruz, CA, USA) was incubated with the nuclear extract for 30 min on ice, then incubated with 80 fmol ^{32}P-labelled oligonucleotide for 30 min on ice before analysis on a 6% polyacrylamide gel. Double-stranded EMSA probes were: CD30-MS1, 5′-CCATCCATCCATCACCTTATGCATCCATCCAT-3′; $CCAT_{12}$, 5′-ATTCCCATCCATCCATCCATCCATCC-ATCCATCCATCCATCCATCCATCCATCG-3′; Sp1-1, 5′-GTTCCTCAAATCCGGGGCGGGCCATTCAA-ACAG-3′; Myc, 5′-GGAAGCAGACCACGTGGTC-TGCTTCC-3′.

Two-dimensional EMSA complex identification

The proteins binding to the double-stranded $(CCAT)_{12}$ probe were analysed previously to determine the molecular mass and the pI of the major CD30-MS EMSA activity d, and identified by analysis on a two-dimensional (2D) IEF/SDS–PAGE gel and silver staining [20]. A second gel, run under identical conditions was stained using 0.1% Coomassie brilliant blue G-250. Spots corresponding to those seen on the silver stained gel in quadrants shown to have EMSA activity, were excised, renatured, recovered from the gel and subjected to MALDI–TOF mass spectrometry, as described previously [20].

One-hybrid cloning and screening

A yeast one-hybrid library was screened essentially as described by the manufacturer (Clontech Inc.). Twelve copies of the CCAT sequence was synthesized with *Eco*RI-compatible ends and inserted in the *Eco*RI cloning site of the pHISi reporter vector (Clontech). The reporter was integrated into the genome of yeast strain, YM4271 (Clontech), grown on solid SD media without histidine, and tested for 3-aminotriazole (3-AT) sensitivity. A concentration of 60 mM 3-AT suppressed growth and was used for subsequent selection. A pACT2-based activation domain fusion library (Human Leukaemia MATCHMAKER cDNA library, Clontech) was transformed into the reporter strain and grown for 4 days at 30 °C on SD medium without

leucine and histidine but containing 60 mM 3-AT. A total of 1.7×10^6 clones were screened. Colonies were assessed for growth by measuring the diameter after 4 days of growth, picked, and the cDNA clone isolated. Isolated plasmids were sequenced. cDNAs from which each clone was derived was identified by comparison with the NCBI human genome database.

Chromatin immunoprecipitation (ChIP)

ChIP was performed using the Chromatin Immunoprecipitation Assay Kit (EZ-Chip™, Upstate Biotechnology, Lake Placid, NY, USA). Karpas-299 cells (1×10^6) were treated with 1% formaldehyde and the remainder of the protocol performed according to the manufacturer's directions, with a minor alteration, ie the addition of 800 µl ChIP dilution buffer to the sample prior to sonication. Lysates were sheared to lengths of 500–1000 base pairs (bp) before diluting with ChIP dilution buffer to 2 ml. The extract was pre-cleared with salmon sperm DNA/protein A agarose, then incubated with 10 µg YY1 antibody (Santa Cruz) at 4 °C overnight. DNA–protein complexes with protein A beads were sequentially washed, eluted, crosslinks reversed and ethanol-precipitated. Input DNA and immunoprecipitated DNA were assayed by PCR (see below) for CD30-MS.

Quantitative RT–PCR of CD30 mRNA

Total RNA (5.0 µg) was used for reverse transcription with Superscript II (Invitrogen). qPCR of CD30, C-MYC and β-actin cDNA was performed using the QuantiTect SYBR Green kit (Qiagen Pty Ltd, Doncaster, Australia) and the following primers: CD30Ex3F, 5′-CGACCGCTGTACAGCCTGCGTGACTTG-3′; CD30Ex5R, 5′-GGAAGCCGGCTCACAGACCGTGTTCTTC-3′; β-actinF, 5′-GCCAACACAGTGCTGTCTGG-3′; β-actinR, 5′-TACTCCTGCTTGCTGATCCA-3′. Reaction mixtures contained 10 µl 2× QuantiTect SYBR Green PCR Master Mix, 0.3 µM each of the forward and reverse primers and an aliquot representing 400 ng input RNA in 20 µl. Quantitative PCR was performed on a Rotor-Gene 3000 (Corbett Research, Sydney, Australia). For the generation of the standard curve, RT–PCR products for CD30 and β-actin were prepared using the Pfx DNA polymerase kit (Invitrogen) and serially diluted (10^{-2} to 10^{-12}). The relative amount of cDNA in each sample was measured by interpolation in the standard curve, and CD30:β-actin expression ratios were calculated.

Laser-capture microdissection and genotyping

Lymph node biopsies were obtained from archived material (PathWest Laboratory Medicine, Perth, Australia) from biopsies characterized as ALK-positive ALCL according to the WHO classification scheme [21] and were used under Australian National Health and Medical Research Council Human Ethics guidelines. Frozen sections were stained using a mouse antihuman CD30 antibody (Ki-1, DAKO, Carpinteria, CA, USA) and rabbit anti-mouse HRP-conjugated immunoglobulin (DAKO). Cells were isolated by laser-assisted microdissection, using a PALM Robot-CombiSystem (PALM Microlaser Technologies GmbH, Bernried, Germany). Samples were digested with 200 µg/ml Proteinase K (Roche Diagnostics Pty. Ltd., Castle Hill, Australia) at 55 °C for 2 h and used directly for PCR typing. The genotyping of the CD30 microsatellite region was performed as described [18].

Results

Activity of CD30 promoter transcriptional reporters in CD30$^+$ lymphoma lines

Previous results indicated that the microsatellite region upstream of the *CD30* gene repressed transcription in reporter gene assays in the CD30$^+$ Jurkat T cell line [14]. To determine whether this region acted similarly in cell lines derived from ALCL biopsies, reporter constructs, either with or without the CD30-MS, were tranfected into Karpas-299, SR-786 or L-428 cells. The results showed that complete deletion of the microsatellite region from the full-length −3.5 kb reporter caused a four-fold increase in activity in all cell lines (Figure 1). The presence of only a $(CCAT)_4$ sequence (construct ΔMS) had a significant negative effect (two-fold) on activity compared to shorter constructs. As previously described, the region between −90 and −40 contained critical transcriptional control elements in the ALCL lines.

One-hybrid analysis of transcription factors interacting with the CD30 microsatellite

The CD30 microsatellite is of the general form $(CCAT)_5$ CACCTTATGCAT$(CCAT)_2$. Previous EMSA analysis indicated that the CCAT sequences in CD30-MS are responsible for binding nuclear factors, rather than the core CACCTTATGCAT sequence of the repeat unit [14]. A one-hybrid bait consisting of 12 CCAT repeat units was cloned into the pHISi one-hydrid vector (Figure 2A). The suitability of the bait sequence was confirmed by EMSA, showing that the complexes which formed on the $(CCAT)_{12}$ sequence were quantitatively the same as those forming on the CD30 repeat unit sequence (Figure 2B). In particular, the major complex, d, appeared identical. Competition reactions confirmed that the complexes had similar affinities for the two probe sequences.

The pHISi-CCAT bait vector was integrated into the host strain YM4721 and transformed with a GAL4 activation domain cDNA library derived from Jurkat T cells. Due to the leaky HIS3 expression, only colonies attaining a diameter of 2.5 mm or more after 4 days of growth were isolated and retested on the selective medium (Figure 2C). Five colonies showing

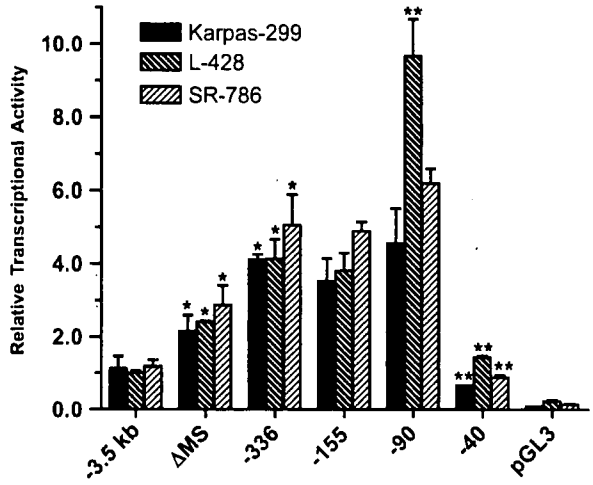

Figure 1. Activity of CD30 promoter transcriptional reporters in ALCL cell lines. Relative CD30 promoter activity was measured in L-428 Hodgkin's and Karpas-299 or SR-786 ALCL cell lines. Cells were transiently transfected with either the full-length CD30 promoter–luciferase reporter construct containing 3.5 kb of upstream sequence (−3.5 kb) or constructs carrying 5′ deletions. ΔMS refers to a construct that carries a deletion of almost all of the CD30-MS, except for four copies of CCAT. The remaining deletion constructs are denoted as a number (in bp) that represents the position of the 5′ deletion end points in relation to the major transcription initiation site (+1). Constructs are described in detail in [14]. For comparison, activity from the parent reporter vector pGL3-basic (pGL3) is shown. Transfected cells were incubated for 24 h and harvested for use in luciferase assays. Relative CD30 promoter activity is expressed as firefly luciferase activity normalized to the respective *Renilla* luciferase activity. The data obtained from at least three independent experiments were analysed for statistical significance using log-transformed data in one-way analysis of variance (ANOVA). Data are presented as mean values ± SEM. Activities found to be significantly different to that of the next longest construct in the same cell line are indicated by asterisks: $^{*}p < 0.01$; $^{**}p < 0.001$

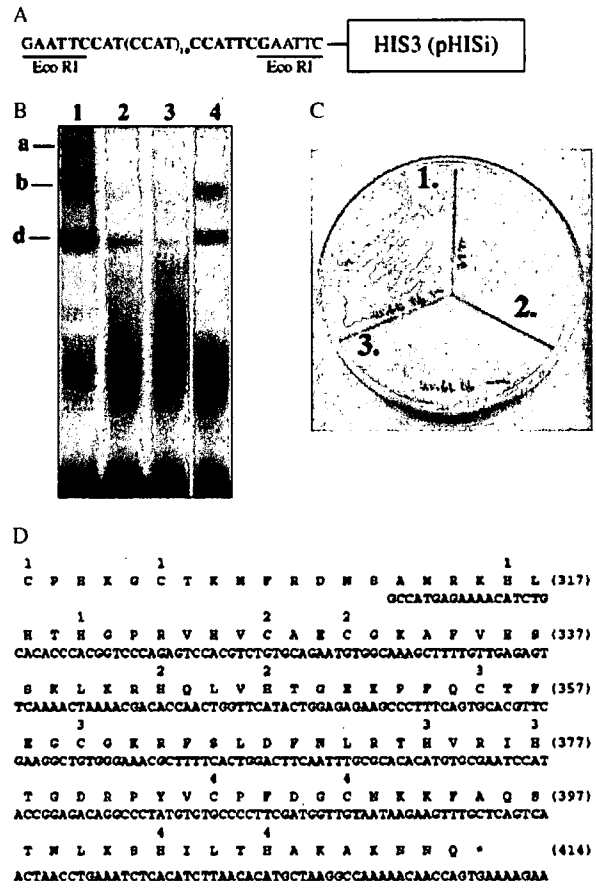

Figure 2. One-hybrid analysis of transcription factors interacting with the CD30 microsatellite. (A) Sequence of the bait region oligonucleotide $CCAT_{12}$ (shown in bold) inserted into the pHISi one-hybrid vector via the *Eco*RI cloning site. (B) EMSA of the CD30-MS using S300 fractionated Jurkat nuclear extract that showed peak activity for complex d and the $CCAT_{12}$ sequence as the labelled probe. In lane 1, previously identified complexes are labelled a, b and d. In addition, lane 2 contains a 50-fold excess, lane 3 a 10-fold excess and lane 4 a five-fold excess of unlabelled CD30-MS1 oligonucleotide as competitor. (C) Selection of positive one-hybrid clones on selective media containing 60 mM 3-AT for 3 days. Sector 1 shows growth of positive clone 17 (YY1). Sector 2 shows background growth of yeast stran YM4271, carrying the integrated CD30-MS/pHISi reporter. Sector 3 shows growth of the parental YM4271 yeast strain. (D) Nucleotide sequence obtained from positive clone 17. Above the sequence is shown the amino acid sequence (414 residues) of human YY1 (NCBI Accession No. NP_003394). The numbers above the sequence mark each of the cysteine (C) or histidine (H) residues that define one of the four C_2H_2 zinc finger motifs found in YY1

the most vigorous growth were analysed. Sequencing of the cDNA inserts isolated from these colonies (see Table 1) showed that in three cases they encoded metabolic enzymes, one containing a sequence of unknown function and one encoding the carboxy-terminal region of the transcription factor Yin Yang 1 (YY1) [22,23]. The cDNA encoded almost the entire DNA binding domain of YY1, consisting of C_2H_2-type zinc fingers 2, 3 and 4 and half of zinc finger 1 (Figure 2D). The results indicated that YY1 was able to bind to the $(CCAT)_{12}$ sequence. Comparison of this sequence with the consensus YY1 binding site, (Cg/a)C/t/a)CATN(Tgc), where CCAT and ACAT were the most common core sequences [24], suggests that YY1 is able to recognize and bind to the CCAT repeat sequence.

Identification of CD30-MS binding activities by peptide mass fingerprinting

As a complement to the one-hybrid analysis, the identity of the major EMSA activity d (see Figure 2B), interacting with the CD30 promoter microsatellite, was determined using an approach we developed recently that utilizes a 2D gel-separation approach [20]. We established that the protein in complex d was approximately 58 kDa, with a pI of 5.8 [20]. Nuclear extract fractions containing complex d activity were subjected to 2D gel electrophoresis, silver-stained, and the region of the second-dimension gel that contains proteins of 58 kDa with a pI of 5.8 were identified (Figure 3A). Four protein spots were observed in this region of the gel. A second gel was run under identical conditions. The three protein spots nearest

Table 1. Identities of one-hybrid cDNA clones

Colony number	cDNA sequence identified	Accession No.
17	*Homo sapiens* Yin Yang 1 (YY1) transcription factor	NM 003403
15	*Homo sapiens* homologue of yeast long chain polyunsaturated fatty acid elongation enzyme 2 (HELO)	AF231981
23	*Homo sapiens* chromosome 17, clone hRPC.4_G_17	AC003688
28	*Homo sapiens* NADH dehydrogenase flavoprotein 3	NM 021075
16	*Homo sapiens* nemo-like kinase	BC064663

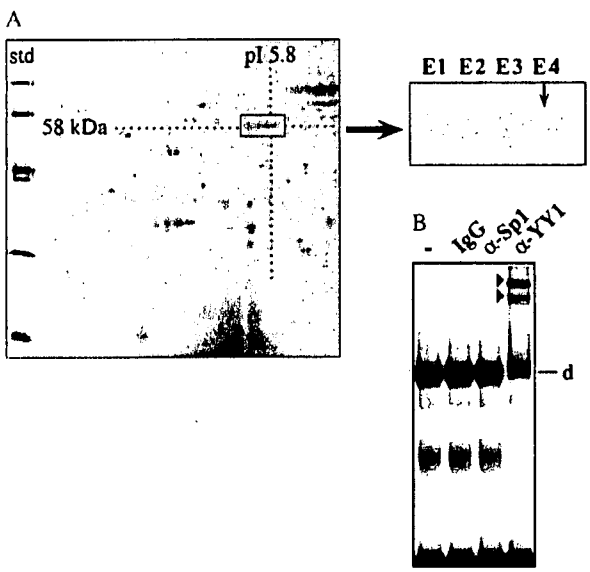

Figure 3. Identification of CD30 microsatellite EMSA-binding activities. (A) 2D IEF/SDS–PAGE gel of S300 fractionated Jurkat nuclear extract was silver-stained and used to identify spots in the region of the gel that conformed to a molecular size of 58 kDa and a pI of 5.8 and showed EMSA activity upon renaturation (see [20]). A second gel was run under identical conditions and stained with Coomassie brilliant blue G-250. Major spot E4 (arrow) and spots E2 and E3 were excised from the gel, digested with trypsin and subjected to peptide mass fingerprinting. (B) Supershift EMSA analysis of the major CD30-MS binding activity, complex d. All EMSA reactions contained 1 μg S300 fractionated Jurkat nuclear extract and labelled CD30-CCAT oligonucleotide probe. The reaction in the last lane contained antibody against YY1; negative control reactions contained either no antibody, non-specific immunoglobulin IgG or antibody against transcription factor Sp1, as indicated. The positions of the YY1-supershifted complexes are indicated by the arrowheads. The DNA–protein EMSA complexes labelled a, b and d are those originally shown to form on the CD30-MS promoter element [14]

to the 58 kDa–pI5.8 intersection (Figure 3A) were excised from the gel and subjected to MALDI–TOF mass spectrometry. Only spots E2 and E4 yielded useful spectral data, which, when used to interrogate the SWISS-PROT and TrEMBL databases via MS-FIT [25], indicated that spot E4 was YY1 (see [20]). Some spot E2 peptide masses also matched YY1, although the sample was heavily contaminated with keratin. To confirm that complex d binding to the CCAT microsatellite sequence contained YY1, EMSA supershift analysis was carried out. The results indicated that YY1-specific antibody was able to supershift complex d, confirming that complex d was composed of YY1 (Figure 3B).

Regulation of *CD30* gene transcription by YY1

To establish that YY1 interacted with the CD30-MS *in vivo*, ChIP was done using Karpas-299 cells. A YY1-specific antibody was able to precipitate the CD30-MS (Figure 4A), indicating that YY1 bound to the MS sequence *in vivo*. To further investigate the role of YY1 in repressing CD30 expression via interaction with the CD30-MS sequences, reporter gene constructs, either with or without CCAT sequences present, were used to test the effect of decreasing YY1 concentration via siRNA-mediated knockdown in CD30 promoter reporter gene assays (Figure 4B). The results indicated that YY1-specific siRNA duplexes served to increase expression of CD30 promoter constructs that contained 3.5 kb of CD30 promoter sequences, including the CD30-MS (−3.5 kb)l; thus, YY1 was acting as a transcriptional repressor. Likewise, the reporter containing a single $(CCAT)_4$ repeat showed a two-fold increase in reporter activity following YY1 siRNA treatment, compared to the GFP siRNA control. The CD-90 reporter containing minimal CD30 promoter sequences but, lacking the CD30-MS entirely, did not show any significant effect of YY1 siRNA treatment over that of the control (Figure 4B), indicating that YY1 was specifically acting through the CD30-MS sequence. Also, the results confirm that $(CCAT)_4$ alone was necessary and sufficient to maximally repress CD30 transcription [14]. The role of YY1 in the regulation of the endogenous *CD30* gene was established following siRNA-mediated 'knockdown' of YY1 in Karpas-299 cells; surface CD30 expression was increased (Figure 4C), indicating that YY1 was acting as a repressor of *CD30* gene transcription.

Comparison of *CD30* mRNA levels and EMSA binding activities in ALCL and HL cell lines

To determine whether there was a correlation between expression levels of CD30 and transcription factor binding activity, particularly activity associating with the MS sequence, we quantitated *CD30* mRNA levels in ALCL (Karpas-299, SR-786, SU-DHL-1) and HL (HDLM2, KMH2, L-540) cell lines and compared this with MS binding activity in EMSA. Real-time PCR analysis of CD30 mRNA levels in the lines (Figure 5A) indicated that the HL-derived line L-540 expressed at the highest level compared to the lowest-expressing cell line, Karpas-299, which expressed at a 10-fold lower level. The other lines expressed at

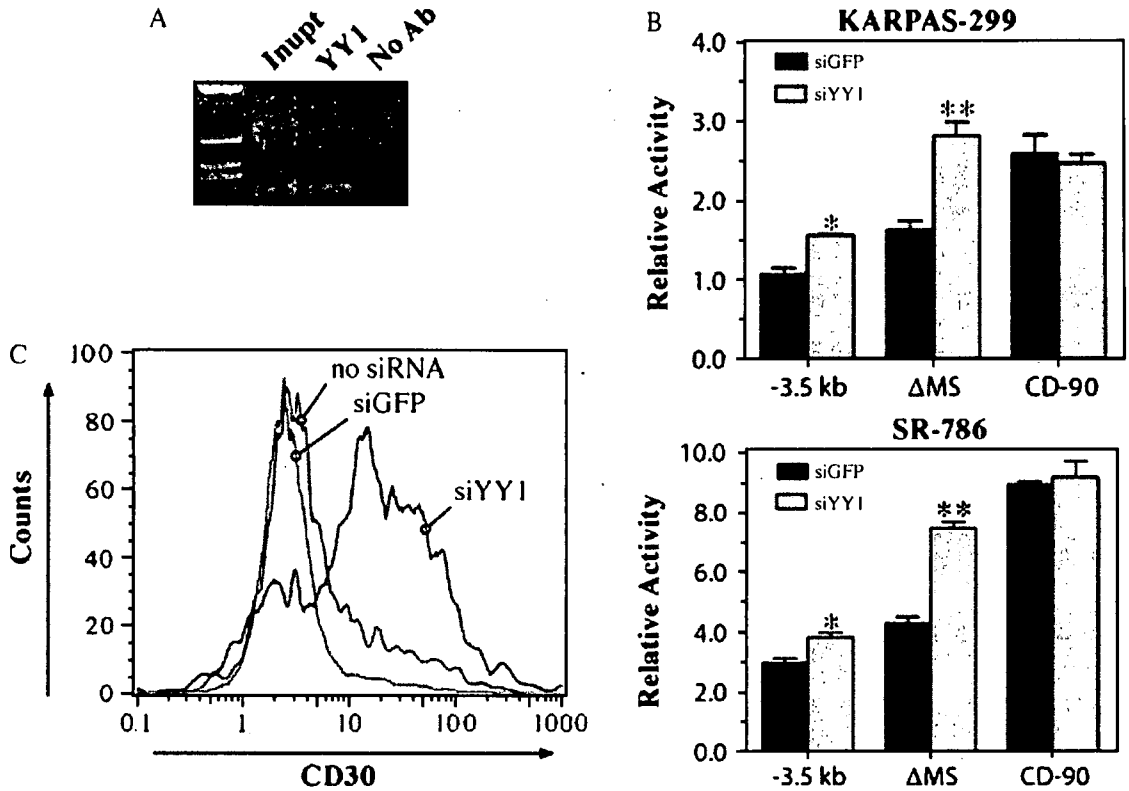

Figure 4. Functional interactions of YY1 with the CD30-MS. (A) ChIP analysis of the CD30-MS was carried out in Karpas-299 cells and the presence of precipitated CD30-MS sequences detected by PCR and agarose gel analysis, as shown. The input reaction contained total genomic DNA from Karpas-299, the ChIP reaction (α-YY1) contained 10 μg supershift YY1 antibody, and the no-antibody (No Ab) control contained 10 μg pre-immune rabbit immunoglobulin. (B) The effects of YY1-specific siRNA on expression of CD30 promoter reporter constructs were measured following tranfection into Karpas-299 or SR-786 cells. Cells were co-transfected with both reporter DNA and fluorescently labelled siRNA specific for YY1 or negative control GFP. Transfection efficiency was assessed by counting fluorescent cells and luciferase activity normalized and plotted as 'relative activity'. The data presented are mean values (± SEM) of three independent transfections. Significant differences between the siGFP control and siYY1 for each reporter construct are indicated (*$p < 0.05$; **$p < 0.005$; Student's *t*-test). (C) The effect of siRNA-mediated 'knock-down' of YY1 on surface expression of CD30 in Karpas-299 was determined by flow cytometry, following transfection with either control siRNA against GFP (siGFP), siRNA against YY1 (siYY1) or untransfected (no siRNA). Cells that had taken up the siRNA were selected by gating on Cy3 fluorescence and levels of CD30 expression determined after staining with PE-conjugated, mouse anti-CD30 monoclonal antibody (BD Biosciences Inc). Flow cytometry was done on a FACScan (Becton-Dickinson, CA, USA)

an intermediate level. All NHL lines expressed *CD30* mRNA at a significantly higher level than the lymphocytic leukaemia line Jurkat. Assessment of the transcription factor binding activities in each cell line was carried out using double-stranded oligonucleotides, whose sequence corresponded to the *cis*-elements found to be important in controlling CD30 expression in the Jurkat cell line [14], the upstream CCAT MS sequence and the Sp1 site at position −43 to −38 (Figure 5B). The results showed that the activities interacting with the Sp1 site did not significantly vary between the cell lines. For the MS repeat sequence, although the levels of binding activity varied substantially between the different lines (Figure 5B), there was no obvious relationship between levels of YY1 binding activity and *CD30* mRNA expression (Figure 5A). These results suggest that differences in expression of CD30 were not due to differences in YY1 or Sp1 transcription factor DNA-binding activity in the cell lines.

Instability of the CD30-MS sequence in ALCL

Previous results in HL cell lines indicated that, although the CD30-MS was unstable, the differences in sequence length were small [19]. To assess the degree of instability in ALCL lines, DNA from Karpas-299 and SU-DHL-1 was subjected to CD30-MS Genescan analysis, as described previously [17,18]. The results indicated that the degree of heterogeneity in both cell lines was greater than that previously found in HL [Figure 6A, panels (a), (b)]. Although major, presumably germ-line MS lengths were present, numerous smaller products were also seen, indicating a shortening of the CD30-MS in a significant proportion of the total cell population.

To exclude the possibility that the heterogeneity in the cell lines was an artefact due to prolonged growth in cell culture, we also determined whether the CD30-MS sequence showed instability in the atypical $CD30^+$ cells of ALCL *in vivo*. Individual $CD30^+$ cells

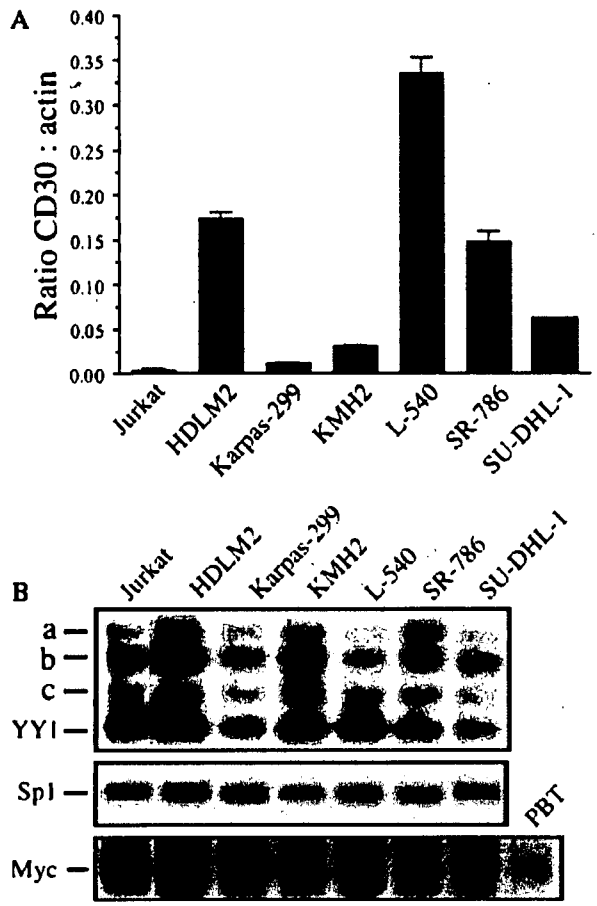

Figure 5. Comparison of *CD30* mRNA levels and EMSA-binding activities in ALCL and HL cell lines. (A) *CD30* mRNA levels in different lymphoma cell lines are expressed as a ratio of *CD30* mRNA expression relative to β-actin expression. Mean levels of expression (± SEM) were derived from quadruplicate real-time PCR measurements. The means for all cell lines were signficantly different (one-way ANOVA, $p < 0.05$). (B) The lymphoma cell line panel was assessed for YY1- and Sp1-binding activity by EMSA, as indicated, using crude nuclear extracts and the probe CD30-MS1 containing the total repeat unit, and the Sp1-1 probe. Also shown is the myc-binding activity (E-box probe) in each cell line compared to peripheral blood T cells (PBT). The unidentified DNA–protein EMSA complexes labelled a, b and c are those originally shown to form on the CD30-MS promoter element [14]

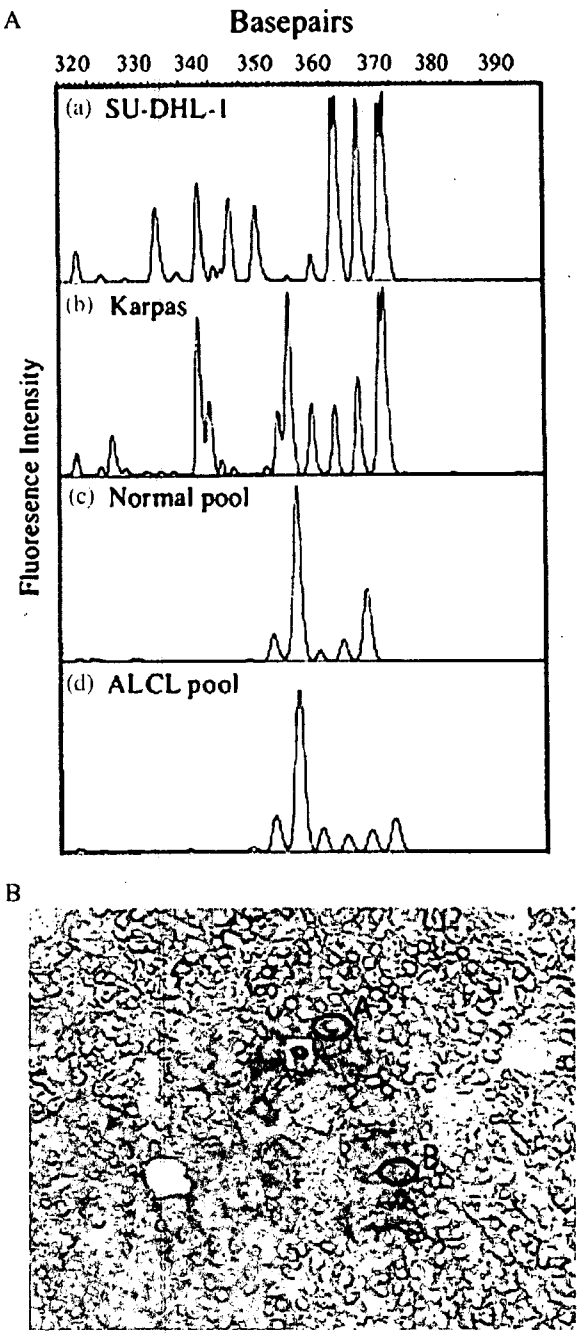

Figure 6. Analysis of CD30-MS sequence length in ALCL cell lines and laser-captured cells in ALCL biopsies. (A) CD30-MS lengths in SU-DHL-1 and Karpas-299 cell lines and in pools of 20 laser-captured, $CD30^+$ ALCL cells or surrounding normal cells from lymph nodes, were determined by Genescan analysis (ABI). PCR primers were HEX-labelled and the PCR products were analysed on a ABI 3100 Genetic Analyser. GeneScan-500 ROX Size Standard was used to size the products. The data were analysed using the program GeneScan Analysis 3.1.2. (B) CD30 immunocytochemical staining of an ALCL lymph node biopsy. Dark areas represent CD30 positivity. Original magnification, ×50. The area marked A represents a captured cell that carried a large deletion of approximately 180 nucleotides (Table 2, patient H, genotype 195/–). For this cell, there was no obvious increase in the intensity of CD30 antibody staining compared to the captured $CD30^+$ cell delineated in area B, showing a 369/377 CD30-MS genotype

from lymph node biopsies of three patients were isolated by laser capture microdissection and subjected to PCR and Genescan analysis (Table 2). Comparison of the CD30-MS genotype from single cells with the patients' genotypes derived from normal tissue or blood indicated that, for both $CD30^+$ and $CD30^-$ lymphocytes, CD30-MS lengths were heterogeneous and in most cases different from the patients' constitutive genotypes. Most of the differences were small and were consistent with the deletion or insertion of a small number of nucleotides. However, in one case a large deletion of approximately 180 nucleotides was observed in one cell (Table 2, patient H) and confirmed by sequencing to be a deletion in the CD30 microsatellite. However, for this cell there was no

Table 2. CD30 genotyping in lymph node biopsies

Patient ID	Genotype
D	373/373 (Genomic DNA)
	373/–(CD30$^+$)
	365/–(CD30$^+$)
	373/377 (CD30$^+$)
	373/377 (CD30$^+$)
S	358/362 (Genomic DNA)
	377/–(CD30$^+$)
	369/–(CD30$^-$)
H	369/373 (Genomic DNA)
	195/–(CD30$^+$)
	369/377 (CD30$^+$)
	316/365/369 (CD30$^+$)
	365/369 (CD30$^+$)
	373/377 (CD30$^-$)
	373/377 (CD30$^-$)
	369/–(CD30$^-$)
	373/377 (CD30$^-$)
	369/373 (CD30$^-$)
	369/377 (CD30$^-$)
	369/377 (CD30$^-$)

obvious increase in CD30 antibody staining compared to other captured CD30$^+$ cells in the surrounding ALCL tissue (Figure 6B).

We also compared a pool of 20 laser-captured CD30$^+$ anaplastic large cells obtained from one biopsy with an equivalent number of normal cells from the surrounding solid tissue [Figure 6A, panels (c), (d)]. The normal cell pool showed two major peaks, of 359 and 371 bp, with characteristic PCR 'stutter' peaks, one and two tetranucleotide repeat units shorter, indicating a genotype of 359/371. In contrast, the ALCL cell pool displayed the 359 allele and associated 'stutter' peaks, but the 371 allele was not predominant and an additional peak of 376 bp was present, indicating a lengthening of the CD30-MS in a significant proportion of cells. Also, the sizes of the presumptive stutter peaks were not consistent with them being by-products of amplication of the 371 bp allele, and indicated the presence also of shortened versions of the CD30-MS in some cells.

Discussion

This study sought to elucidate the nature of the upstream events that lead to very high CD30 expression in ALCL. Previously we described a tetranucleotide repeat element in the CD30 promoter that represses transcription. In the current study, we have identified the transcriptional repressor YY1 as the mediator of this repression. YY1 is a ubiquitous protein that appears to have many roles in regulating gene expresssion and can act as either a repressor or an activator, depending on the cellular context [26,27]. YY1 associates with many transcriptional activators and co-regulators, including TBP, TFIIB [28,29], Sp1 [30], AP2 [31], retinoblastoma (Rb) [32] and p300 [33]. Of relevance to CD30 expression in lymphoma, YY1 associates with the proto-oncogene *C-MYC* [34]. Although our data indicate that YY1 DNA binding activity is not elevated in ALCL, we have confirmed (Figure 5B) that myc levels are elevated in ALCL cells [35–37]. The *C-MYC* interaction domain of YY1 has been mapped and shown to be the same as that which interacts with TBP and TFIIB [28,29]; thus, the interaction of YY1 with *c-myc* may serve to block the transcriptional repression (or activation) activity but not the DNA-binding activity of YY1. These data suggest a model in which YY1, bound to the upstream CD30 microsatellite sequence, normally exerts its effect by interacting with TBP and/or TFIIB to modulate transcription. However, in the presence of *c-myc* binding, the normal interactions with the preinitiation complex are blocked, thus inhibiting YY1 activity. The high levels of c-Myc in ALCL cells may have the effect of lessening the repressive activity of YY1, leading to elevated CD30 expression. We also have shown recently that fos/JunB is able to relieve the YY1-mediated repression of the *CD30* gene [19]. Presumably this occurs through an interaction with YY1. Both of these mechanisms may operate in parellel, resulting in the very high levels of CD30 expression seen on ALCL cells.

Our data indicate that the CD30-MS exhibits instability, usually of small insertions or deletions of the repeat unit. However, these differences do not correlate with the level of CD30 expression or with CD30 expression at all. Our previous results suggest that deletion of almost the entire repeat sequence is necessary to elicit a significant increase in CD30 transcriptional activity [14]. However, in the present study, in only one case was a significant shortening of the CD30 microsatellite seen, suggesting that deletion is a possible, but rare, mechanism for upregulating CD30 expression. We conclude that CD30-MS length *per se* is not a major driver of increased CD30 expression in ALCL.

The role of YY1 in regulating CD30 expression has significant implications, due to its function as a chromatin interactor and modifier [38,39]. This point of control provides a potential avenue for therapeutic intervention, through the use of histone deacetylase inhibitors and other agents that interfere with the normal interactions of transcription factors and co-factors. There is some evidence that the cell surface levels of CD30 may be important in dictating the cellular response after binding of the ligand CD153. Some studies have indicated that apoptosis or cell cycle arrest ensues, whereas others have documented activation or proliferation signals [9,10]. These ostensibly conflicting data can be explained if the nature of the response in ALCL cells is dependent on CD30 receptor density on the cell surface [40]. Low receptor density could allow anti-proliferative or apoptotic signals to predominate, resulting in tumour regression. High receptor density might allow proliferative signals to

predominate, leading to tumour growth. Thus, therapeutic intervention at the level of CD30 expression is a strategy that may prove useful in the treatment of ALCL.

Acknowledgements

This work was supported by generous funding from the Cancer Council, Western Australia, and the Raine Medical Research Foundation. We thank Evelyn Susanto for one-hybrid library screening.

References

1. Schwab U, Stein H, Gerdes J, Lemke H, Kirchner H, Schaadt M, *et al.* Production of a monoclonal antibody specific for Hodgkin and Sternberg–Reed cells of Hodgkin's disease and a subset of normal lymphoid cells. *Nature* 1982;**299**:65–67.
2. Stein H, Gerdes J, Schwab U, Lemke H, Mason DY, Ziegler A, *et al.* Identification of Hodgkin and Sternberg–Reed cells as a unique cell type derived from a newly-detected small-cell population. *Int J Cancer* 1982;**30**:445–459.
3. Stein H, Foss HD, Durkop H, Marafioti T, Delsol G, Pulford K, *et al.* CD30$^+$ anaplastic large cell lymphoma: a review of its histopathologic, genetic, and clinical features. *Blood* 2000;**96**:3681–3695.
4. Ansieau S, Scheffrahn I, Mosialos G, Brand H, Duyster J, Kaye K, *et al.* Tumor necrosis factor receptor-associated factor (TRAF)-1, TRAF-2, and TRAF-3 interact *in vivo* with the CD30 cytoplasmic domain; TRAF-2 mediates CD30-induced nuclear factor kappa B activation. *Proc Natl Acad Sci USA* 1996;**93**:14053–14058.
5. Gedrich RW, Gilfillan MC, Duckett CS, Van Dongen JL, Thompson CB. CD30 contains two binding sites with different specificities for members of the tumor necrosis factor receptor-associated factor family of signal transducing proteins. *J Biol Chem* 1996;**271**:12852–12858.
6. Bargou RC, Emmerich F, Krappmann D, Bommert K, Mapara MY, Arnold W, *et al.* Constitutive nuclear factor-kappaB–RelA activation is required for proliferation and survival of Hodgkin's disease tumor cells. *J Clin Invest* 1997;**100**:2961–2969.
7. Mir SS, Richter BW, Duckett CS. Differential effects of CD30 activation in anaplastic large cell lymphoma and Hodgkin disease cells. *Blood* 2000;**96**:4307–4312.
8. Horie R, Watanabe M, Ishida T, Koiwa T, Aizawa S, Itoh K, *et al.* The NPM–ALK oncoprotein abrogates CD30 signaling and constitutive NF-κB activation in anaplastic large cell lymphoma. *Cancer Cell* 2004;**5**:353–364.
9. Pfeifer W, Levi E, Petrogiannis-Haliotis T, Lehmann L, Wang Z, Kadin ME. A murine xenograft model for human CD30$^+$ anaplastic large cell lymphoma. Successful growth inhibition with an anti-CD30 antibody (HeFi-1). *Am J Pathol* 1999;**155**:1353–1359.
10. Mori M, Manuelli C, Pimpinelli N, Mavilia C, Maggi E, Santucci M, *et al.* CD30–CD30 ligand interaction in primary cutaneous CD30$^+$ T cell lymphomas: a clue to the pathophysiology of clinical regression. *Blood* 1999;**94**:3077–3083.
11. Nagata S, Ise T, Onda M, Nakamura K, Ho M, Raubitschek A, *et al.* Cell membrane-specific epitopes on CD30: potentially superior targets for immunotherapy. *Proc Natl Acad Sci USA* 2005;**102**:7946–7951.
12. Zhang M, Yao Z, Zhang Z, Garmestani K, Goldman CK, Ravetch JV, *et al.* Effective therapy for a murine model of human anaplastic large-cell lymphoma with the anti-CD30 monoclonal antibody, HeFi-1, does not require activating Fc receptors. *Blood* 2006;**108**:705–710.
13. Croager EJ, Muir TM, Abraham LJ. Analysis of the human and mouse promoter region of the non-Hodgkin's lymphoma-associated *CD30* gene. *J Interferon Cytokine Res* 1998;**18**:915–920.
14. Croager EJ, Gout AM, Abraham LJ. Involvement of Sp1 and microsatellite repressor sequences in the transcriptional control of the human *CD30* gene. *Am J Pathol* 2000;**156**:1723–1731.
15. Durkop H, Oberbarnscheidt M, Latza U, Bulfone-Paus S, Hirsch B, Pohl T, *et al.* The restricted expression pattern of the Hodgkin's lymphoma-associated cytokine receptor CD30 is regulated by a minimal promoter. *J Pathol* 2000;**192**:182–193.
16. Durkop H, Oberbarnscheidt M, Latza U, Bulfone-Paus S, Krause H, Pohl T, *et al.* Structure of the Hodgkin's lymphoma-associated human *CD30* gene and the influence of a microsatellite region on its expression in *CD30*$^+$ cell lines. *Biochim Biophys Acta* 2001;**1519**:185–191.
17. Franchina M, Kadin ME, Abraham LJ. Polymorphism of the CD30 promoter microsatellite repressive element is associated with development of primary cutaneous lymphoproliferative disorders. *Cancer Epidemiol Biomarkers Prev* 2005;**14**:1322–1325.
18. McIntyre MQ, Price P, Franchina M, French MA, Abraham LJ. Distribution of human *CD30* gene promoter microsatellite alleles in healthy and human immunodeficiency virus-1 infected populations. *Eur J Immunogenet* 2003;**30**:125–128.
19. Watanabe M, Ogawa Y, Ito K, Higashihara M, Kadin ME, Abraham LJ, *et al.* AP-1 mediated relief of repressive activity of the CD30 promoter microsatellite in Hodgkin and Reed–Sternberg cells. *Am J Pathol* 2003;**163**:633–641.
20. Woo AJ, Dods JS, Susanto E, Ulgiati D, Abraham LJ. A proteomics approach for the identification of DNA binding activities observed in the electrophoretic mobility shift assay. *Mol Cell Proteomics* 2002;**1**:472–478.
21. Jaffe ES, Harris NL, Stein H, Vardiman JWE. *WHO Classification of Tumours. Pathology and Genetics of Tumours of Haematopoietic and Lymphoid Tissues*. IARC Press: Lyon, France, 2001.
22. Park K, Atchison ML. Isolation of a candidate repressor/activator, NF-E1 (YY-1 delta), that binds to the immunoglobulin kappa 3′ enhancer and the immunoglobulin heavy-chain mu E1 site. *Proc Natl Acad Sci USA* 1991;**88**:9804–9808.
23. Shi Y, Seto E, Chang LS, Shenk T. Transcriptional repression by YY1, a human GLI–Kruppel-related protein, and relief of repression by adenovirus E1A protein. *Cell* 1991;**67**:377–388.
24. Hyde-DeRuyscher RP, Jennings E, Shenk T. DNA binding sites for the transcriptional activator/repressor YY1. *Nucleic Acids Res* 1995;**23**:4457–4465.
25. Clauser KR, Baker P, Burlingame AL. Role of accurate mass measurement (±10 p.p.m.) in protein identification strategies employing MS or MS/MS and database searching. *Anal Chem* 1999;**71**:2871–2882.
26. Galvin KM, Shi Y. Multiple mechanisms of transcriptional repression by YY1. *Mol Cell Biol* 1997;**17**:3723–3732.
27. Shi Y, Lee JS, Galvin KM. Everything you have ever wanted to know about Yin Yang 1. *Biochim Biophys Acta* 1997;**1332**:49–66.
28. Austen M, Luscher B, Luscher-Firzlaff JM. Characterization of the transcriptional regulator YY1. The bipartite transactivation domain is independent of interaction with the TATA box-binding protein, transcription factor IIB, TAFII55, or cAMP-responsive element-binding protein (CPB)-binding protein. *J Biol Chem* 1997;**272**:1709–1717.
29. Usheva A, Shenk T. TATA-binding protein-independent initiation: YY1, TFIIB, and RNA polymerase II direct basal transcription on supercoiled template DNA. *Cell* 1994;**76**:1115–1121.
30. Lee JS, Galvin KM, Shi Y. Evidence for physical interaction between the zinc-finger transcription factors YY1 and Sp1. *Proc Natl Acad Sci USA* 1993;**90**:6145–6149.
31. Begon DY, Delacroix L, Vernimmen D, Jackers P, Winkler R. Yin Yang 1 cooperates with activator protein 2 to stimulate *ERBB2* gene expression in mammary cancer cells. *J Biol Chem* 2005;**280**:24428–24434.
32. Petkova V, Romanowski MJ, Sulijoadikusumo I, Rohne D, Kang P, Shenk T, *et al.* Interaction between YY1 and the retinoblastoma protein. Regulation of cell cycle progression in differentiated cells. *J Biol Chem* 2001;**276**:7932–7936.
33. Lee JS, Galvin KM, See RH, Eckner R, Livingston D, Moran E, *et al.* Relief of YY1 transcriptional repression by adenovirus

E1A is mediated by E1A-associated protein p300. *Genes Dev* 1995;**9**:1188–1198.
34. Shrivastava A, Saleque S, Kalpana GV, Artandi S, Goff SP, Calame K. Inhibition of transcriptional regulator Yin-Yang-1 by association with c-Myc. *Science* 1993;**262**:1889–1892.
35. Jack AS, Kerr IB, Evan G, Lee FD. The distribution of the *c-myc* oncogene product in malignant lymphomas and various normal tissues as demonstrated by immunocytochemistry. *Br J Cancer* 1986;**53**:713–719.
36. Mitani S, Sugawara I, Shiku H, Mori S. Expression of *c-myc* oncogene product and *ras* family oncogene products in various human malignant lymphomas defined by immunohistochemical techniques. *Cancer* 1988;**62**:2085–2093.
37. Raetz EA, Perkins SL, Carlson MA, Schooler KP, Carroll WL, Virshup DM. The nucleophosmin-anaplastic lymphoma kinase fusion protein induces c-Myc expression in pediatric anaplastic large cell lymphomas. *Am J Pathol* 2002;**161**:875–883.
38. Satijn DP, Hamer KM, den Blaauwen J, Otte AP. The polycomb group protein EED interacts with YY1, and both proteins induce neural tissue in *Xenopus* embryos. *Mol Cell Biol* 2001;**21**:1360–1369.
39. Thomas MJ, Seto E. Unlocking the mechanisms of transcription factor YY1: are chromatin modifying enzymes the key? *Gene* 1999;**236**:197–208.
40. Franchina M, Karimi M, Ho D, Abraham LJ. Effects of CD30 receptor density on intracellular signalling: insights into anaplastic large cell lymphoma treatment. Proceedings of the 6th International Cytokine Society Conference 2006: 55–59. In *6th International Cytokine Conference; 2006*. Medimond Srl: Vienna, Austria, 2006; 55–59.

THE JOURNAL OF BIOLOGICAL CHEMISTRY VOL. 282, NO. 18, pp. 13875–13883, May 4, 2007

The Nuclear Import of the Human T Lymphotropic Virus Type I (HTLV-1) Tax Protein Is Carrier- and Energy-independent*

Received for publication, December 19, 2006, and in revised form, March 6, 2007 Published, JBC Papers in Press, March 6, 2007, DOI 10.1074/jbc.M611629200

Takahiro Tsuji[‡], Noreen Sheehy[‡], Virginie W. Gautier[‡], Hitoshi Hayakawa[‡], Hirofumi Sawa[§], and William W. Hall[‡1]

From the [‡]Centre for Research in Infectious Disease, School of Medicine & Medical Science, University College Dublin, Belfield, Dublin 4, Ireland and the [§]Department of Molecular Pathobiology and 21st Century COE Program for Zoonosis Control, Hokkaido University Research Center for Zoonosis Control, N18, W9, Kita-ku, Sapporo, 060-0818, Japan

HTLV-1 is the etiologic agent of the adult T cell leukemia-lymphoma (ATLL). The viral regulatory protein Tax plays a central role in leukemogenesis as a transcriptional transactivator of both viral and cellular gene expression, and this requires Tax activity in both the cytoplasm and the nucleus. In the present study, we have investigated the mechanisms involved in the nuclear localization of Tax. Employing a GFP fusion expression system and a range of Tax mutants, we could confirm that the N-terminal 60 amino acids, and specifically residues within the zinc finger motif in this region, are important for nuclear localization. Using an *in vitro* nuclear import assay, it could be demonstrated that the transportation of Tax to the nucleus required neither energy nor carrier proteins. Specific and direct binding between Tax and p62, a nucleoporin with which the importin beta family of proteins have been known to interact was also observed. The nuclear import activity of wild type Tax and its mutants and their binding affinity for p62 were also clearly correlated, suggesting that the entry of Tax into the nucleus involves a direct interaction with nucleoporins within the nuclear pore complex (NPC). The nuclear export of Tax was also shown to be carrier independent. It could be also demonstrated that Tax it self may have a carrier function and that the NF-κB subunit p65 could be imported into the nucleus by Tax. These studies suggest that Tax could alter the nucleocytoplasmic distribution of cellular proteins, and this could contribute to the deregulation of cellular processes observed in HTLV-1 infection.

Human T cell lymphotropic virus type-I (HTLV-1)[2] is the etiologic agent of the malignant disorder adult T cell leukemia-lymphoma (ATLL) (1, 2). Whereas the pathogenesis of ATLL is unclear, the HTLV-1 regulatory protein Tax is thought to play a central role in leukemogenesis. Tax has been shown to immortalize human T cells (3) and transform fibroblast cells (4) *in vitro*, and transgenic animals expressing Tax have developed a range of malignancies (5–8). The mechanisms of the transformation are not fully understood, but have been shown to be related to the ability of Tax to dysregulate the transcription of genes involved in cellular proliferation, cell-cycle control, and apoptosis (9–11). Tax is a potent transcriptional transactivator not only of viral but also of cellular gene expression. The protein physically interacts with a number of cellular transcription factors, which including components of the NF-κB-Rel signaling complex, and persistent and constitutive activation of NF-κB is central to the development and maintenance of the malignant phenotype in ATLL (10–12).

Activation of NF-κB involves Tax activity in both the cytoplasm and nucleus. In the cytoplasm, Tax activates the kinase activity of IKK complex by directly interacting with IKKγ/NEMO subunit. IκBα, which sequesters NF-κB in the cytoplasm, is phosphorylated by the Tax-IKK complex and subsequently degraded allowing the nuclear translocation of NF-κB (13). In the nucleus, Tax has also been shown to co-localize with NF-κB as well as basic transcriptional factors such as p300/CBP in nuclear speckle structures, the so-called Tax speckle structure (TSS), where active transcription of a range of cellular genes occurs (14, 15).

Consistent with both its cytoplasmic and nuclear activities, Tax has been shown to be distributed in both compartments in HTLV-1-infected and Tax-transfected cells. In initial studies, Tax was reported to be found predominantly in the nucleus and specifically accumulated in the nuclear speckled structures (16, 17). However, depending on the cell type, significant amounts of Tax have also been found in the cytoplasm (18–20). Specifically, cytoplasmic Tax was shown to co-localize in the endoplasmic reticulum, Golgi apparatus, and mitotic organizing center (MTOC), and appeared to affect both protein secretion and microtubule organization (21, 22). Recent studies employing a heterokaryon fusion system have also clearly demonstrated that Tax can effectively shuttle between the cytoplasm and the nucleus (18).

Nuclear transport of proteins occur through the nuclear pore complex (NPC), and in most cases involves an interaction between transport carriers and a nuclear localization signal (NLS) on the cargo protein (23, 24). Most transport carriers belongs to the importin (karyopherin) family and mediate transport either as monomers and heterodimers. Importin α/β heterodimers import cargo proteins containing a "classical" NLS which is generally rich in lysine residues (23). Importin β monomer imports a range of cargo proteins including the parathyroid hormone-related protein (25), the sterol regulatory

* The costs of publication of this article were defrayed in part by the payment of page charges. This article must therefore be hereby marked "*advertisement*" in accordance with 18 U.S.C. Section 1734 solely to indicate this fact.

[1] To whom correspondence should be addressed. Tel.: 353-1-716-1229; Fax: 353-1-716-1239; E-mail: william.hall@ucd.ie.

[2] The abbreviations used are: HTLV-1, human T cell lymphotropic virus type-I; GST, glutathione *S*-transferase; WGA, wheat germ agglutinin; GFP, green fluorescent protein; MAPK, mitogen-activated protein kinase; TSS, Tax speckle structure; NPC, nuclear pore complex; ATLL, adult T cell leukemia-lymphoma; RRL, rabbit reticulocyte lysate; DAPI, 4′,6-diamidino-2-phenylindole; WT, wild type.

element-binding protein 2 (SREBP-2) (26), the zinc finger protein Snail (27), as well as the viral proteins HIV-1 Rev (28, 29) and HTLV-1 Rex (30). Transportin monomer, which also belongs to the importin β family, imports cargo proteins such as hnRNP A1 protein (31), several kinds of histones (32) and ribosomal proteins (33). The import process requires metabolic energy and is propelled by a concentration gradient across the nuclear envelope of the GTP-bound form of small GTPase Ran, which is found at high concentrations in the nucleus (23). In contrast, the transport of a number of other proteins is carrier independent; these include β-catenin (34), MAPK (35, 36), SMAD (37), STAT (38), HIV-1 Vpr (39), RCC1 (40), and PU.1 (41) all of which have been shown to translocate through the nuclear pore complex (NPC) in the apparent absence of a carrier protein.

While the N-terminal ~60 amino acids of Tax has been shown to be important for the nuclear localization of Tax (42–44), there is no similarity between the amino acid sequences in this region and those of the other NLSs so far reported, and the mechanism by which Tax is transported into the nucleus has remained unclear. In the present study, we have analyzed the nuclear import of Tax using an *in vitro* nuclear import assay system which allows manipulation of the soluble components and selective reconstitution of the nuclear import process *in vitro* using exogeneous substrates. Our results demonstrate that Tax is imported into the nucleus through the NPC by directly interacting with components of the NPC and this is both energy independent and does not require a carrier protein. Notably our studies also show that Tax itself may function as a carrier protein permitting the nuclear translocation of a number of cellular proteins and this may in turn contribute to the dysregulation of cell function which occurs in HTLV-1 infection.

EXPERIMENTAL PROCEDURES

Cell Culture and Transfection—HeLa and COS7 cells were maintained in Dulbecco's minimal essential medium supplemented with 10% fetal bovine serum and penicillin/streptomycin. HeLa cells were plated on 18-well printed slides (Roboz Surgical Instrument Co., Inc., Gaithersburg, MD) for the *in vitro* nuclear import assays 24 h before the experiments. COS7 cells were plated on two-well chamber slides (Nalge Nunc International, Naperville, IL) 24 h before transfection. Cells were transfected with 1 μg of plasmids using FuGENE6 (Roche Diagnostics, Mannheim, Germany).

DNA Construction and Plasmids—To create mammalian expression vectors for GFP-Tax/-Tax340/-Tax220/-Tax116/-Tax60/-Tax55/-Tax50, cDNA sequences encoding full-length Tax and the series of C-terminal deletion mutants were amplified by PCR and cloned into the HindIII/PstI sites of the pEGFP-C1 vector (Clontech).

The bacterial expression vectors for the SV40 T antigen NLS, GST-SV40TNLS-GFP (pGEX-SV40TNLS-GFP), GST-HA-importin β (pGEX-HA-importin β), GST-importin β (pGEX-importin β), and His_6-RanQ69L (pQE80-RanQ69L) were gifts from Dr. S. Kose and Dr. N. Imamoto (RIKEN, Saitama, Japan). To create the bacterial expression vectors for GST-Tax-GFP and GST-Tax340-GFP, the SV40-T-antigen NLS coding sequences of pGEX-SV40TNLS-GFP were swapped for the Tax and Tax1–340 coding sequences by utilizing BamHI/SmaI sites of the vector. To create bacterial expression vectors for GST-Tax340-CFP and GST-YFP-Rev, Tax1–340, and CFP encoding sequences from pECFP-C1 (Clontech) were cloned into the BamHI and SmaI sites of pGEX-2T vector (Amersham Biosciences), and YFP encoding sequences from pEYFP-C1 (Clontech) and HIV-1 Rev encoding sequences were cloned into the SmaI and EcoRI sites of pGEX-2T vector. To construct bacterial expression vector for GST-Tax, Tax encoding sequences were cloned into the BamHI site of pGEX-2T vector. The bacterial expression vectors for GST-p62FL [1–522], GST-p62N [1–265] and GST-p62C [178–522] were generated by cloning relevant sequences (41) from pcDNA3.1/His-p62 vector (a gift from Dr. N. Yaseen, Northwestern University, Chicago, IL) into pGEX-2T vector. To construct the bacterial expression vector expressing His_6-p65-YFP, p65 encoding sequencing amplified from pcDNA-p65 vector (a gift from Dr. D. Walls, Dublin City University, Dublin, Ireland) and YFP encoding sequences amplified from pEYFP-C1 (Clontech) vector were cloned into the BamHI and PstI sites of pQE80 (Qiagen) vector. QuikChange™ site-directed mutagenesis kit (Stratagene) was used for the creation of single amino acid mutations in Tax-encoding sequences.

Expression and Purification of Recombinant Proteins—All GST and His fusion proteins were purified from *Escherichia coli* strain BL21(DE) induced with 0.5 mM isopropyl-β-D-thiogalactopyranoside for 14 h at 18 °C. Purifications were performed on glutathione-Sepharose 4B beads (Amersham Biosciences) for the GST fusions and on Ni-NTA agarose beads (Qiagen) for the His fusions, according to the manufacturer's protocols. Tax-/TaxC23A-/TaxC29A-/TaxC36A-/TaxH41A-GFP, Tax340-GFP/-CFP, and HA-importin β were cleaved from GST by using thrombin. To obtain RanQ69L-GTP, 2 mM EDTA, 2 mM GTP, and 5 mM $MgCl_2$ were added to His_6-RanQ69L, which had been eluted from resin and incubated for 30 min on ice. All resultant proteins were dialyzed against transport buffer (TB; 20 mM HEPES, pH7.3, 110 mM potassium acetate, 2 mM magnesium acetate, 5 mM sodium acetate, 0.5 mM EGTA, 2 mM dithiothreitol, 1 μg/ml aprotinin, leupeptin, and pepstatin A), and concentrated by ultrafiltration on Microcon (Amicon), and stored at −80 °C after snap freezing.

In Vitro Nuclear Transport Assay—In vitro nuclear import assays were performed essentially as described previously (34, 45). HeLa cells plated on glass slides were washed twice with ice-cold TB and permeabilized with digitonin (40 μg/ml, Sigma) in TB for 5 min on ice. Cells were then washed twice with ice-cold TB and soaked in TB for 10 min on ice. The standard reaction mixtures contained import substrates (~1 μM), an ATP regeneration system (1 mM ATP, 5 mM phosphocreatine, 20 units of creatine kinase) as a source of energy, and rabbit reticulocyte lysate (RRL, Promega) as a source of soluble import factors. The import reaction was performed for 20 min at 30 °C or on ice. For the export reactions, the cells initially subjected to the import reaction were immediately washed twice with TB and then were incubated with testing solutions for 20 min at 30 °C to examine export. The composition of each of the reaction mixtures are described in each figure legend. After the

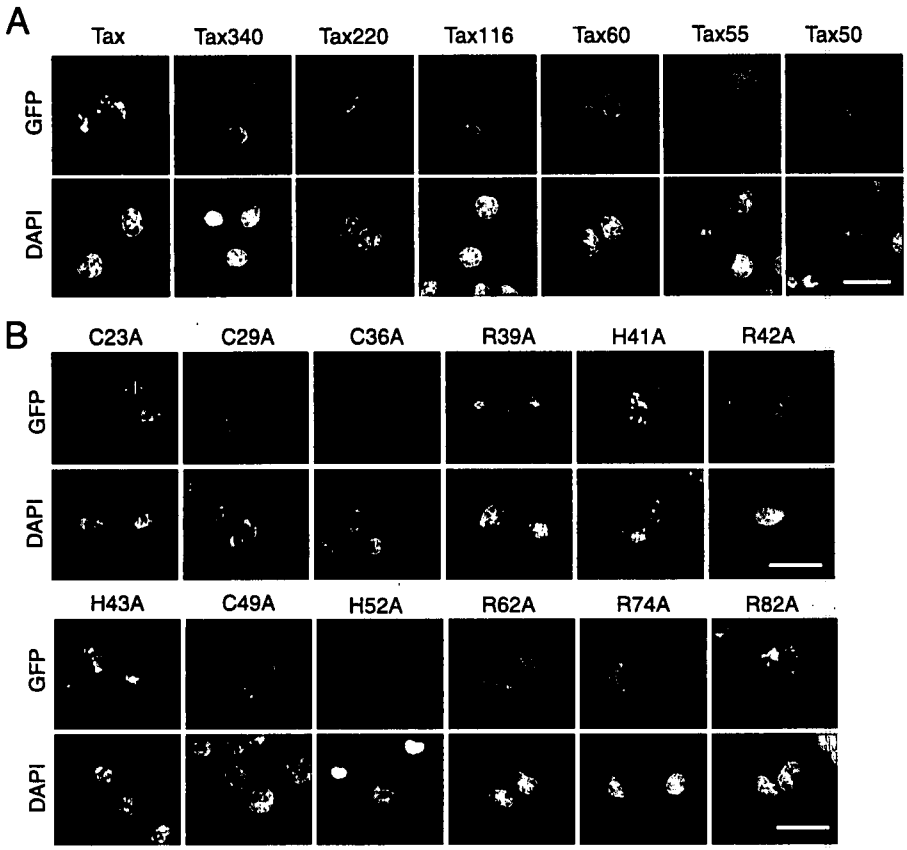

FIGURE 1. **The N-terminal 60 amino acids of Tax are necessary for the nuclear localization of Tax.** COS7 cells were transiently transfected with GFP-Tax and GFP-Tax-C-terminal deletion mutants (*A*) or GFP-Tax with single amino acid mutants (*B*). Twenty-four hours later, cells were fixed and counterstained with DAPI. Representative images of transfected cells were demonstrated. *Scale bars*, 20 μm.

transport reactions, the cells were washed twice with TB followed by fixation with 4% paraformaldehyde for 8 min at room temperature. The cells were washed twice with TB and mounted with 50% glycerol in TB, and examined by fluorescence microscopy. Fluorescent intensities in nuclei and in randomly chosen areas outside the nuclei were quantified by using ImageJ software (NIH).

Protein Binding Assay—Recombinant GST or GST fusion proteins were incubated with HA-importin β or GFP fusion proteins in a total volume of 100 μl in TB with 3% bovine serum albumin. After incubation for 20 min at room temperature, 10 μl of glutathione-Sepharose 4B beads were added to the reaction mixtures and incubated for 30 min at room temperature. The bead complexes were then washed four times with 500 μl each of TB. Bound proteins were eluted from the beads with 25 μl of 10 mM reduced glutathione and analyzed by SDS-PAGE and immunoblotting. In immunoblotting, rabbit anti-GFP antibody (ab290, Abcam, UK) and mouse anti-HA antibody (HA-7, Sigma) were used, and the antibody detection was performed using the Superfemto chemiluminescent kit (Pierce).

RESULTS

The N Terminal 60 Amino Acids Are Important for the Nuclear Accumulation of Tax—Tax has been known to localize primarily in the nucleus in HTLV-1-infected or Tax-transfected cells (15,16,22,42–44,46). The 60 amino acids of the N terminus of Tax have been shown to be necessary for its nuclear localization, as fusion of this region permits nuclear localization of heterogeneous proteins, and deletion of the region results in the complete loss of Tax nuclear localization (42–44).

To confirm and extend these findings, we employed a GFP fusion protein system as this has been widely utilized in subcellular localization analyses of a number of proteins including Tax (19, 20, 47). DNA fragments encoding a full-length Tax or a series of C-terminal deletion mutants of Tax were inserted into the C terminus of a GFP expression vector, and their subcellular localizations were examined (Fig. 1*A*). As previously reported, GFP with full-length Tax localized both in the nucleus and in the cytoplasm with a speckled pattern (Fig. 1*A*) (20, 21). GFP with C-terminal deletions (Tax340, Tax220, Tax116, and Tax60 and as well as Tax280; Fig. 1*A*, and not shown) accumulated almost exclusively in the nucleus. Of note, Tax340, a mutant with the deletion of only the C-terminal 13 amino acids, completely lost its cytoplasmic localization pattern. Tax C-terminal deletion mutants shorter than Tax60 resulted in the leakage of the fusion protein into the cytoplasm (Tax55 and Tax50 as well as Tax45; Fig. 1*A*, and not shown). Therefore, as has been previously shown (42–44), it could be confirmed that the N-terminal 60 amino acids of Tax were the minimal region permitting the localization of the GFP fusion protein to the nucleus.

To determine which single amino acids may be critical for the nuclear localization of Tax, the subcellular localization of single amino acid mutants of GFP-Tax were examined (Table 1 and Fig. 1*B*). We focused on the zinc finger like motif between amino acids 23–52 and the basic amino acid cluster between 39–43, because these motifs are potential binding sites for importin β (23, 27, 28, 30, 48). Site directed mutagenesis of these amino acids were carried out. Among 20 mutants generated, 5 mutants (C29A, C36A, R42A, C49A, H52A) within the N-terminal 60 amino acids exhibited a dominant distribution in the cytoplasm (Table 1 and Fig. 1*B*). Taken together, our data confirm that the zinc finger motif within the N-terminal 60 amino acids is important for the nuclear localization of Tax.

Tax Enters the Nucleus by an Energy- and Carrier-independent Mechanism—To investigate the mechanisms by which Tax is transported into the nucleus, an *in vitro* nuclear import assay using digitonin-permeabilized cells was carried out (45).

Proteins larger than 40 kDa are generally transported through the NPC by an active and receptor-mediated mechanism (49). The import substrates used in these studies were full-length Tax, and the C-terminal deletion mutant Tax fused with GFP at their C terminus (Tax-GFP and Tax340-GFP) both of which are ~66 kDa in size and which would not be expected to enter the nucleus by a passive diffusion. GST-SV40TNLS-GFP was employed as a control carrier-dependent import substrate. In the complete assay system, which contained both cytosol and energy, all three substrates were efficiently imported into the nucleus (Fig. 2*A*, *panels a*, *d*, and *g*). Wheat germ agglutinin (WGA) binds to glycosylated nucleoporins and blocks nuclear transport mediated via the NPC (50, 51). In cells treated with WGA, none of the substrates accumulated in the nucleus (Fig. 2*A*, *panels b*, *e*, and *h*). Nuclear import was also inhibited by "on-ice" incubation (Fig. 2*A*, *panels c*, *f*, and *i*). These results indicate that the nuclear import of Tax-GFP and Tax340-GFP are carried out by an active transport mechanism through the active transport channels of the NPC, and not by passive diffusion.

TABLE 1
Subcellular localization of GFP-Tax with single amino acid mutation

Mutation	Subcellular localization
C23A	WT[a]
C29A	C[b]
C36A	C
R39A	WT
H41A	WT
R42A	C
H43A	WT
C49A	C
H52A	C
R62A	WT
R74A	WT
R82A	WT
K85A	WT
K88A	WT
R110A	WT
H127A	WT
C153A	WT
C174A	WT
R190A	WT

[a] WT, the localization of the mutant is similar to that of GFP with wild type Tax.
[b] C, the mutant localizes predominantly in the cytoplasm.

To further characterize the nuclear import of Tax, the effects of the depletion of energy or cytosol from import mixtures were examined. The depletion of energy markedly inhibited the nuclear import of GST-SV40TNLS-GFP but had no effect on the nuclear import of Tax-GFP and Tax340-GFP (Fig. 2*B*, *panels b*, *f*, and *j*). Interestingly, Tax340-GFP was imported into the nucleus even in the absence of cytosol. In contrast, Tax-GFP was found also to preferentially localize to the nuclear membrane and did not have such a clear cut distribution within the nucleus compared with the C-terminal deletion mutant (Fig. 2*B*, *panels c* and *g*). To investigate the effect of Ran on the nuclear import of Tax, RanQ69L, a mutant Ran which is deficient in GTP hydrolysis was added to the import mixture (Fig. 2*B*, *panels d*, *h*, and *l*). RanQ69L effectively inhibited the nuclear accumulation of GST-SV40TNLS-GFP, but not that of Tax-GFP and Tax340-GFP. These results indicate that Tax can enter the nucleus without energy or carriers including the importin β family proteins, which are known to require the GTPase activity of Ran for carrier function (23).

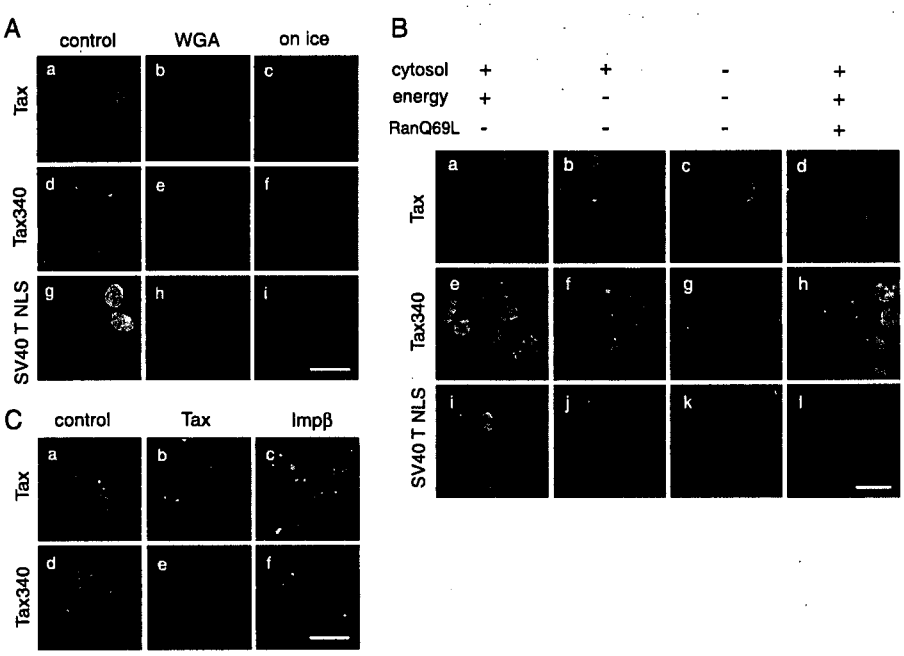

FIGURE 2. **The nuclear import of Tax is carried out by a facilitated process that is independent of energy and carriers.** The nuclear import of Tax-GFP (*Tax*), Tax340-GFP (*Tax340*), and GST-SV40TNLS-GFP (*SV40 T NLS*) were examined by *in vitro* nuclear import assay. *A*, digitonin-permeabilized HeLa cells were incubated with 10 μl of reaction mixtures containing 0.3 μM of an import substrate, ATP regeneration system, and rabbit reticulocyte lysate. Permeabilized cells were pretreated with 0.5 mg/ml WGA (Sigma) for 10 min at room temperature (*panels b*, *e* and *h*). The import reactions were performed at on ice instead of 30 °C (*panels c*, *f* and *i*). *B*, digitonin-permeabilized HeLa cells were incubated with 10 μl of reaction mixtures containing 0.3 μM of import substrate. To eliminate triphosphoric acids, the reaction mixtures were preincubated in the presence of 0.1 units/ml apyrase (Sigma) for 5 min at 30 °C prior to the reactions of energy-free conditions (*panels b*, *c*, *f*, *g*, *j*, and *k*). 5 μM RanQ69L-GTP were included in the reactions of the +*RanQ69L* condition (*panels d*, *h* and *i*). *C*, compositions of import mixtures were essentially as same as that of *A*, *panels a* and *d*. The import mixtures contained 30 μM GST (*control*, *panels a* and *d*), 30 μM GST-Tax (*Tax*, *panels b* and *e*), and 30 μM GST-importin β (*Impβ*, *panels c* and *f*) as competitors. *Scale bars*, 20 μm.

To determine whether the nuclear entry of Tax involves a facilitated mechanism, *in vitro* nuclear import assays were carried out in the presence of GST-Tax or GST-importin β as unlabeled fluorescent competitors (Fig. 2*C*). Both GST-Tax and GST-importin β reduced the nuclear uptake of Tax-GFP and Tax340-GFP, indicating that the nuclear import of Tax is saturable, and the import involves the specific components of the NPC which are also involved in interactions with importin β.

The Nuclear Import of Tax Involves a Direct Interaction with the FG Repeats of Nucleoporins—As it has been reported that the carrier-independent translocation of proteins into the nucleus involves a

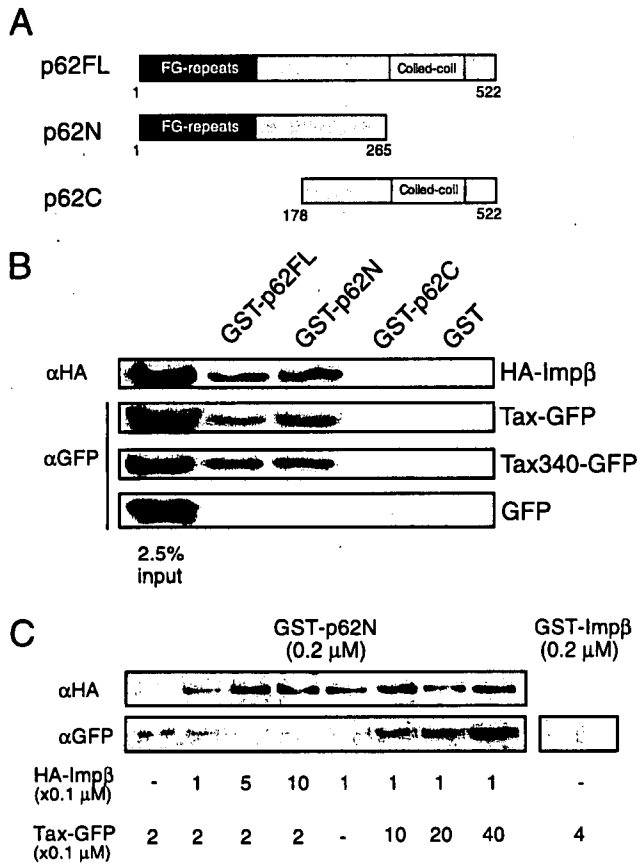

FIGURE 3. **Tax binds directly to the FG repeat region of p62 *in vitro*.** *A*, scheme of *p62FL* and its deletion mutants, *p62N* and *p62C*, which were used in the protein binding assay. *B* and *C*, in protein binding assays, the mixtures of recombinant proteins were allowed to immobilize on glutathione-Sepharose 4B beads, and bound fractions were analyzed by immunoblotting. In *B*, recombinant *GST*, *GST-p62FL*, *GST-p62N*, and *GST-p62C* (0.2 μM each) were mixed and incubated with *HA-Impβ*, *Tax-GFP*, *Tax340-GFP*, or *GFP* (0.2 μM each). To minimize the differences in the elution efficiencies between all GST fusion proteins from the beads, the total volume of the mixtures were increased to 300 μl, and the elution step was carried out three times. In *C*, recombinant GST-p62N was mixed and incubated at the indicated concentrations of *HA-Impβ* and *Tax-GFP*. *FL*, full-length. *Impβ*, importin β.

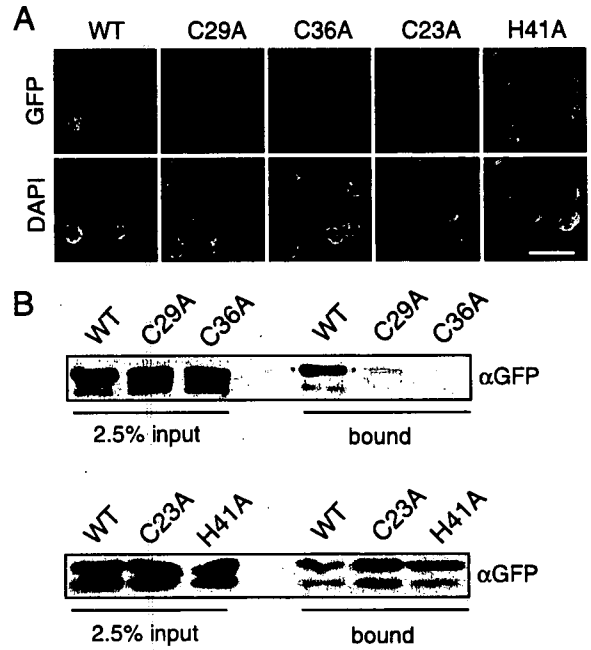

FIGURE 4. **The nuclear import activity of Tax is dependent on the binding of Tax and the FG repeats of nucleoporin.** The recombinant GFP fusions, Tax-GFP (*WT*), TaxC23A-GFP (*C23A*), TaxC29A-GFP (*C29A*), TaxC36A-GFP (*C36A*), and TaxH41A-GFP (*H41A*) were examined by *in vitro* nuclear import assay (*A*) and protein binding assay (*B*). In *A*, the digitonin-permeabilized HeLa cells were incubated with 10 μl of reaction mixtures containing 0.3 μM GFP fusions, ATP regeneration system, and RRL. *Scale bars*, 20 μm. In *B*, GST-p62N (0.2 μM) was mixed and incubated with GFP fusions (0.2 μM each). The reaction mixtures were then allowed to immobilize on glutathione-Sepharose 4B beads, and bound fractions were analyzed by immunoblotting using anti-GFP antibody.

direct interaction(s) between the proteins and nucleoporins within the NPC (23,35–38,52), we investigated whether Tax can also interact with nucleoporins. The FG repeat containing nucleoporins, including p62, Nup153, and Nup214/CAN have been implicated in nuclear import and are also known to interact with several importin β family proteins (reviewed in Ref. 53). To investigate if Tax can interact with nucleoporins, recombinant GST fused with full-length p62 and both C- or N-terminal deletion mutants of this protein were purified and assayed for their binding to Tax-GFP or HA-importin β. The C-terminal deletion mutant of p62 (p62N) contained the FG repeat region, whereas the N-terminal deletion mutant of p62 (p62C) did not (Fig. 3*A*). In control experiments, HA-importin β was found to bind to "full-length" GST-p62FL and to GST-p62N. This was also shown not to bind to GST-p62C or GST itself (Fig. 3*B*). Tax-GFP and Tax340-GFP also specifically bound to GST-p62FL and GST-p62N (Fig. 3*B*, right). Interactions of GFP and GST or GST fusion proteins were not observed. These results clearly show that Tax interacts with the FG repeat region of p62 *in vitro*. Our studies also suggest that Tax340 may bind p62FL with a greater affinity than wild type Tax (Fig. 3*B*). However this remains to be further investigated.

To determine if Tax and importin β compete for the binding to the FG repeats of p62, *in vitro* competition assays were carried out (Fig. 3*C*). Only a 2.5-fold amount of importin β effectively inhibited the binding between Tax and p62. In contrast, as much as a 40-fold amount of Tax did not completely inhibit the binding between importin β and p62. Binding between importin β and Tax was not observed (Fig. 3*C*, *right*). This suggests that Tax and importin β may share common docking sites on the FG repeats of nucleoporins, but the affinity between Tax and p62 is considerably lower than that between importin β and p62. To determine whether the nuclear import activity of Tax is dependent on an interaction between Tax and nucleoporins, the single amino acid Tax mutants, which were found to have lost (C29A and C36A) or retained (C23A and H41A) their nuclear localization properties (Fig. 1*B*), were expressed as GFP fusion proteins, and their nuclear import activity and binding affinity with p62 examined. Among wild type Tax and the four mutants, the nuclear import activities in digitonin-permeabilized cells closely correlated with the binding affinity with p62 (Fig. 4). Specifically these results support the proposal that the nuclear import of Tax requires direct interactions with regions in the nucleoporins containing the FG repeats.

The Nuclear Export of Tax Is Also Carrier- and Energy-independent—A number of studies have shown that certain proteins which enter the nucleus without import carriers (transportin, β-catenin, and MAPK) are also known to exit the nucleus without export carriers (35, 54–56). This raised the possibility that Tax may also exit from the nucleus without export carriers, and to investigate this, we examined the export of Tax using digitonin-permeabilized cells. Cells were firstly incubated with import mixtures containing Tax-GFP, Tax340-GFP, and GST-YFP-Rev as control, and subsequently washed and incubated with export buffer. To identify the components required for nuclear export, the export reactions were carried out with transport buffer (Fig. 5, *panels a*, *d*, and *g*) or buffer containing cytosol and energy (Fig. 5, *panels b*, *e*, and *h*). In addition, the transport buffer containing WGA was used to confirm the integrity of the nuclear membrane structures (Fig. 5, *panels c*, *f*, and *i*). The export of GST-YFP-Rev was observed only in the presence of cytosolic factors and energy, consistent with previous reports that the nuclear export of the HIV-1 Rev was CRM1-dependent (Fig. 5, *panel h*) (57). In contrast, GST-YFP-Rev was not exported from the nucleus under cytosol- and energy-free conditions (Fig. 5, *panel g*). Tax-GFP and Tax340-GFP were efficiently exported under the same conditions (Fig. 5, *panels a* and *d*). Quantification of the export process demonstrated that the export efficiencies of Tax-GFP and Tax340-GFP in the presence of cytosol and energy (Fig. 5, *panels b* and *e*) were almost the same as that in the absence of cytosol and energy (Fig. 5, *panels a* and *d*). These results indicate that Tax is also able to exit the nucleus in an energy- and carrier-independent manner.

Tax Can Transport p65 into the Nucleus—Our results have demonstrated that Tax can enter and exit the nucleus without a carrier protein, and these processes are energy-independent. Moreover, the nuclear import process appears to involve a direct interaction between Tax and the FG repeat regions of nucleoporins. Because these properties are also shared with known import receptors such as the importin β family proteins (58–61), we attempted to determine if Tax can also function as an import receptor. p65, an NF-κB family protein subunit, was chosen as a putative cargo of Tax, because this protein has been shown to be closely associated with Tax both in the cytoplasm and in the nucleus. Specifically, Tax has been associated with the release of p65 from the IκBα-p65 complex in the cytoplasm (13), and Tax and p65 co-localize in the nucleus (14). In addition, physical binding of Tax and p65 has been reported (62, 63). To determine whether p65 can be imported by Tax, p65 fused with YFP (p65-YFP) and Tax340 fused with CFP (Tax340-CFP) were expressed and used as substrates in the *in vitro* nuclear import assay. In the presence of energy and cytosol, p65-YFP was found to be distributed in both the nucleus and cytoplasm (Fig. 6*A*, *panel a*). The nuclear import of p65-YFP was inhibited by the addition of WGA or RanQ69L (Fig. 6*A*, *panels b* and *c*) and by the deprivation of cytosol in the import mixtures (Fig. 6*B*, *panel a*), all of which is consistent with the nuclear import of p65 being carried out by the importin α/β-mediated classical import pathway (64). Tax340-CFP was also expressed, and we confirmed as expected that the nuclear import of Tax340-CFP was a carrier- and an energy-independent process (data not shown). As shown in Fig. 6*B*, even without the addition of cytosolic factors and energy, p65-YFP was localized in the nucleus in the presence of Tax340. Moreover, p65-YFP migrated into the nucleus even in the presence of RanQ69L and cytosol if Tax-CFP was present in the import mixture (data not shown). These results indicate that p65 can migrate into the nucleus not only by the importin α/β import pathway, but also by a Tax-mediated pathway.

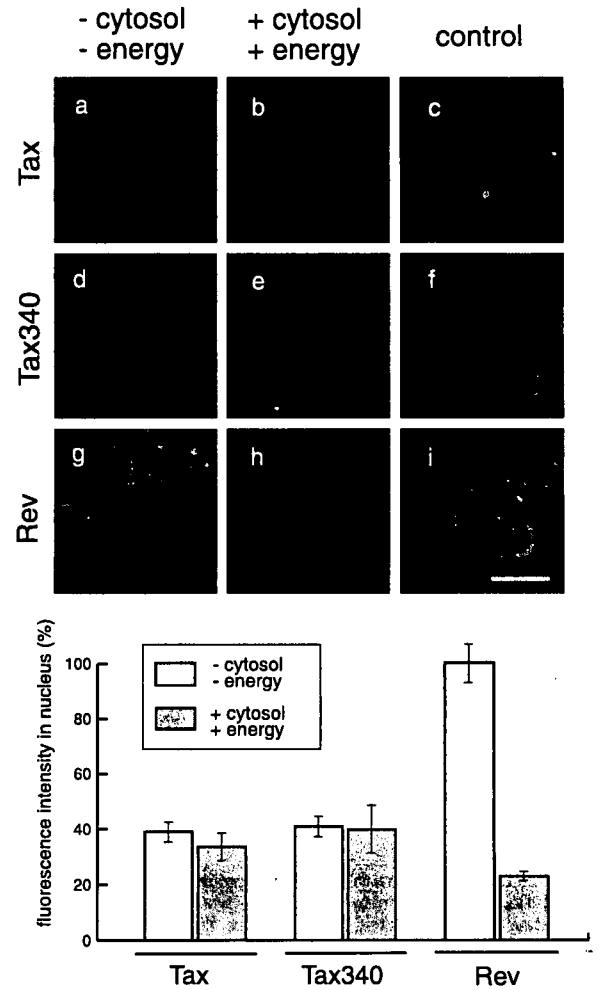

FIGURE 5. **Tax can be exported from the nucleus without carriers and energy.** The nuclear export of Tax-GFP (*Tax*), Tax340-GFP (*Tax340*), and GST-YFP-Rev (*Rev*) were examined. The digitonin-permeabilized HeLa cells were initially incubated with 10 μl of reaction mixtures containing import substrates (0.3 μM Tax-GFP, 0.3 μM Tax340-GFP, or 1.0 μM GST-YFP-Rev), RRL, and the ATP-regeneration system. Cells were then washed and reincubated with transport buffer (*−cytosol −energy*), that containing RRL and the ATP regeneration system (*+cytosol +energy*) or that containing 0.5 mg/ml WGA (*control*) to examine export. To obtain optimal nuclear accumulation of GST-YFP-Rev, all cells were pretreated with 10 nM leptomycin B for 30 min prior to digitonin permeabilization, and 10 nM leptomycin B was also included in the import reaction mixtures. *Graph*, fluorescent intensity of each nucleus was measured after the export reactions. The mean intensity of 30–40 nuclei was drawn. The mean intensity of nuclei incubated in the presence of 0.5 mg/ml WGA was taken as 100%. *Error bars* indicated standard deviation of the results of four independent experiments. *Scale bars*, 20 μm.

DISCUSSION

A number of studies have clearly shown that HTLV-1 Tax protein co-localizes in both the nucleus and the cytoplasm. In

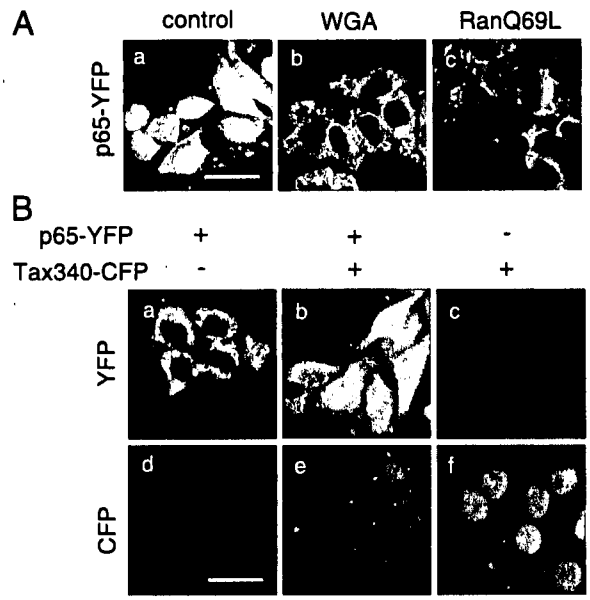

FIGURE 6. **p65 can be imported into the nucleus by Tax.** *A*, nuclear import of p65-YFP was characterized by *in vitro* nuclear import assay. Digitonin-permeabilized HeLa cells were incubated with 10 μl of standard import mixtures containing 0.2 μM p65-YFP, ATP regeneration system, and RRL (*panel a, control*). Before the incubation, permeabilized cells were pretreated with 0.5 mg/ml WGA (Sigma) for 10 min at room temperature (*panel b, WGA*). 5 μM RanQ69L-GTP was included in the standard import mixture (*panel c, RanQ69L*). *B*, the nuclear import of p65-YFP was examined in the absence of cytosol and energy. The import mixtures contained 0.2 μM p65-YFP under the *+p65-YFP* condition (*panels a, b, d,* and *e*), and 0.5 μM Tax340-CFP was under the *+Tax340-CFP* condition (*panels b, c, e,* and *f*). The import mixtures were pretreated with apyrase (0.1 unit/ml) prior to the import reactions. *Scale bars*, 20 μm.

the nucleus, Tax is observed in speckles in the so-called Tax speckle structure (TSS) where it is involved in the transcription of cellular genes through interactions with a number of transcription factors (14–16). In the cytoplasm, in addition to being directly involved with NF-κB activation (reviewed in Ref. 13), Tax co-localizes in several subcellular organelles including the endoplasmic reticulum, the Golgi apparatus, and the microtubule-organizing center (MTOC) and is believed to influence secretion pathways and microtubule organization (21, 22).

In the present study, we have investigated the intracellular localization of Tax and specifically the mechanisms involved in its nuclear localization. These have clearly shown that the nuclear import of Tax is carrier independent. Most proteins are transported into the nucleus by forming complexes with carrier proteins, which belong to importin β families with the carrier-cargo complex subsequently translocating through the NPC (23). However, a number of proteins have been shown to enter the nucleus directly. These include the carrier proteins themselves importin β (59), transportin (54), and importin α (65), as well as β-catenin (34), MAPK (35, 36), SMAD (37), STAT (38), HIV-1 Vpr (39), RCC1 (40) and PU.1 (41). We have also clearly shown that Tax requires neither energy nor Ran for its nuclear import which is a characteristic feature of proteins with a carrier-independent nuclear import (34, 35, 37, 39, 54). A common feature of the carrier-independent process is the direct interaction of proteins with nucleoporins in the NPC (23, 35–38, 41, 52). In the present study, we could also demonstrate a direct interaction between Tax and p62, one of the nucleoporins, which is located in the central plug of the NPC suggesting that Tax also shares this common property. It could be demonstrated using specific Tax mutants that the nuclear import of Tax correlated with the binding to p62 suggesting that this is an essential part of nuclear import. In addition, it could be shown that the nuclear import of Tax was inhibited by an excess amount of importin β, and that the binding between Tax and p62 was blocked by importin β. Taken together, the results suggest that Tax and importin β bind to a common region(s) in the nucleoporins.

Carrier- and energy-independent nuclear transport is thought to be carried out by a process similar to the so-called "facilitated diffusion," which requires specific, but weak interactions between the protein and nucleoporins (40, 66, 67). This sort of transport mechanism involves minimal energy and is thought to be driven by Brownian motion. In the case of β-catenin, the subcellular localization of the protein is thought to be controlled by retention in either the nucleus or the cytoplasm rather than a selective increase of import or export. Specifically, the transcription factors including T-cell factor/lymphocyte enhancer factor (LEF/TCF) and BCL9 or the cytoplasmic proteins including APC and Axin function as nuclear or cytoplasmic retention factors for β-catenin (68). The nuclear localization of MAPK is also thought to be regulated by the nuclear anchor proteins (69). Consistent with this, it is possible that the nuclear localization of Tax might be related to retention caused by Tax-binding proteins in the nucleus such as p65 and CBP, which serve as a bridge between the nucleosome and Tax. Cytoplasmic localization could involve immobile structures such as the MTOC and cytoskeleton to which Tax can bind directly or indirectly. One important observation in our study was that Tax340 was imported into the nucleus efficiently without cytosol and energy, but wild type Tax was imported efficiently only in the presence of cytosol. It is likely that the C-terminal 13 amino acids, which we have shown to be associated with the cytoplasmic distribution of Tax may serve as part of a "cytoplasmic retention signal." In the absence of cytosol, the C terminus of Tax could be sequestered by immobile structures in the cytoplasm, and in the presence of cytosol, Tax would be released from the cytoplasmic retention by the protein binding to the C terminus of Tax and permitting translocation through the NPC. It is also possible that Tax340 may have a greater binding affinity for the NPC compared with wild type Tax facilitating nuclear localization but this will require further detailed investigations. These and other studies are underway to further examine the importance of the C-terminal region in the localization of Tax.

The mechanisms of the nuclear export of Tax also remain to be defined. It was recently shown that under UV stress conditions, Tax was exported from the nucleus by an interaction with the carrier protein CRM1, on the basis that this was inhibited by leptomycin B (70). In contrast, under normal culture conditions, the nuclear export of Tax was found to be insensitive to leptomycin B (20, 70). As we demonstrated that the addition of exogenous transport factor and energy did not facilitate the nuclear export of Tax, it appears that Tax can exit the nucleus in a carrier and energy independent manner and this may account